Cell detoxification of secondary metabolites by P4-ATPase mediated vesicle transport

Yujie Li[1†], Hui Ren[1†], Fanlong Wang[1], Jianjun Chen[1], Lian Ma[1], Yang Chen[1], Xianbi Li[1], Yanhua Fan[1], Dan Jin[1], Lei Hou[1], Yonghong Zhou[1], Nemat O. Keyhani[2], and Yan Pei[1*]

[1]Biotechnology Research Center, Southwest University, Beibei, Chongqing 400715, China; [2]Department of Microbiology and Cell Science, Institute of Food and Agricultural Sciences, University of Florida, Gainesville, FL 32611, USA.

[†]Yujie Li and Hui Ren contributed equally to this work

[*]For correspondence: peiyan3@swu.edu.cn

Abstract

Mechanisms for cellular detoxification of drug compounds are of significant interest in human health. Cyclosporine A (CsA) and tacrolimus (FK506) are widely known antifungal and immunosuppressive microbial natural products. However, both compounds can result in significant side effects when used as immunosuppressants. The insect pathogenic fungus *Beauveria bassiana* shows resistance to CsA and FK506. However, the mechanisms underlying the resistance have remained unknown. Here, we identify a P4-ATPase gene, *BbCRPA*, from the fungus, which confers resistance *via* a unique vesicle mediated transport pathway that targets the compounds into detoxifying vacuoles. Interestingly, the expression of *BbCRPA* in plants promotes resistance to the phytopathogenic fungus *Verticillium dahliae via* detoxification of the mycotoxin cinnamyl acetate using a similar pathway. Our data reveal a new function for a subclass of P4-ATPases in cell detoxification. The P4-ATPases conferred

cross-species resistance can be exploited for plant disease control and human health protection.

Keywords

Beauveria bassiana; P4-ATPase; vesicle transport pathway; vacuole; plant protection

Introduction

The mining of bioactive molecules known as secondary metabolites or natural products is of significant interest relevant to almost all aspects of human activity from food security to health and well-being. Microbes are known reservoirs for the production of such natural products, that has included the discovery of the world's first broad spectrum antibiotic from *Penicillium notatum* to a range of diverse chemical compounds that continue to be characterized from fungi today (Brakhage, 2013; Chanda et al., 2009; Fleming, 1944; Keller et al., 2005). Two of the most widely known microbial products of human health relevance are cyclosporine A (CsA), a neutral lipophilic cyclic polypeptide originally isolated from the entomopathogenic fungus *Beauveria nivea* (*Tolypocladium inflatum*) and FK506 (tacrolimus), a macrolide lactone isolated from *Streptomyces tsukubaensis* (Gupta et al., 1989; Odom et al., 1997; Tanaka et al., 1987). Although both of these molecules were originally isolated due to their antifungal properties, their functioning as immunosuppressive agents has revolutionized aspects of medicine (Borel et al., 1976; Beauchesne et al., 2007; Dreyfuss et al., 1976; Guada et al., 2016; Margaritis and Chahal, 1989; Odom et al., 1997; Tanaka et al., 1987). The major mechanism mediating the antimicrobial activities of both CsA and FK506 appear to be *via* inhibition of calcium signaling by targeting of calcineurin (CaN) through cyclophilin A-CsA and FKBP-FK506 complexes, respectively (Liu et al., 1991; Sharma et al., 1994). In terms of human health relevance, however, CsA and FK506 are highly used immunosuppressants that have been applied in a wide variety of therapeutic applications from facilitating human organ transplants to autoimmune-disease therapies, hypertension, and even ocular diseases (Borel and Gunn, 1986; Thomson et al., 1993; Tory et al., 2008). However, both compounds can also result in significant

side effects that can include nephro- and hepatotoxicities, central nervous system (CNS) disturbances, hirsutism, and gingival hyperplasia (DiMartini et al., 1996; Kaeberlein, 2013). Little, however, is known concerning mechanisms for detoxification of these drugs, and to date no pathways have been identified for mediating (microbial or other) resistance (s) to these compounds. Resistance can be of further importance due to the effects of similar fungal secondary metabolite toxins produced by phytopathogens that cause significant agricultural damage and decreased productivity. Within this context the phyotopathogenic fungi, *Verticillium dahliae Kleb* and *Fusarium graminearum*, causing Verticillium wilt corn ear rot and wheat head blight disease, respectively, are two of the most destructive diseases of many important crops (Subbarao et al., 1995; Sutton, 1982; Veronese et al., 2003), and mycotoxins, such as trichothecenes produced by *F. graminearum*, present in foods and forages cause serious risks to the health of animals and human beings (Berthiller, et al., 2013; D'Mello, et al., 1999).

Most organisms are endowed with two major mechanisms for detoxification of small molecular weight chemical compounds: (i) chemical modification (s) resulting in inactivation, which can include hydrolysis and/or oxidation, and conjugation, (ii) compartmentation, and eventual degradation (Berthiller et al., 2013; Coleman et al., 1997). In compartmental detoxification, molecules (toxins) are transported into structures (organelles) where they are sequestered and degraded. As part of these processes, it had been demonstrated that vesicle-mediated transport can contribute to secondary metabolite sequestering in order to protect the host cell (or resistant organisms) from self-toxicity (Sirikantaramas et al., 2008). In fungi and plants, the primary subcellular compartment for detoxification is the vacuole, while in animals it is the lysosome. It is well known that ATP-binding cassette (ABC) transporters can

78 catalyze drug/toxin efflux across membranes out of cells and/or into specialized
79 compartments as part of mechanisms involved in drug resistance and detoxification
80 (Coleman et al., 1997; Theodoulou, 2000; Sipos and Kuchler, 2006; Wolfger et al.,
81 2001). Most ABC transporters are floppases mediating the movement of
82 phospholipids from the cytosolic surface to the extracellular leaflet (Coleman et al.,
83 2013; Perez et al., 2015; van Meer et al., 2006; Zhou and Graham, 2009). Unlike ABC
84 transporters, type IV P-type ATPases (P4-ATPases) have been proposed to function as
85 phospholipid flippases that pump specific phospholipid substrates in the reverse
86 direction: from the exofacial to the cytosolic leaflet of membranes (Coleman et al.,
87 2013; Hankins et al., 2015; Zhou and Graham, 2009). P4-ATPases, identified only in
88 eukaryotic cells, constitute the largest subfamily of P-type ATPase, and have
89 important roles in the initiation of the vesicle formation and membrane trafficking by
90 the generation of phospholipid asymmetry in biological membranes, which are
91 involved in a variety of physiological processes, including cell surface growth, the
92 biogenesis of cellular organelles, endocytosis, and protein storage and protein sorting
93 (De Matteis et al., 2013; Hara-nishimura et al., 1998; Lopez-Marques et al., 2014;
94 McMahon and Gallop, 2005; Rothman and Wieland, 1996; van der Mark et al., 2013).
95 However, to date the functioning of P4-ATPases in cell detoxification of small
96 peptides and/or secondary metabolites has not been reported.

97 The insect pathogenic fungus *B. bassiana* is resistant to CsA (Zhou et al., 2016). In
98 this study, from a screen of a fungal random insertion mutant library, a *B. bassiana*
99 CsA susceptible mutant was identified. The mutation insertion site was mapped to an
100 open reading frame coding for a P4-ATPase and designated as BbCrpa (cyclosporine
101 A resistance P4-ATPase). The mechanism for BbCrpa functioning is shown to be *via*
102 delivery of the toxins into vacuoles through a P4-ATPase mediated vesicle transport

pathway. Interestingly, the expression of *BbCRPA* in *Arabidopsis thaliana* and *Gossypium hirsutum Linn.* (cotton) significantly increased the resistance of transgenic plants against *V. dahliae* toxin, and reduced the severity of Verticillium wilt disease, indicating the utilization of the P4-ATPase endowed detoxification in other species.

Results

BbCrpa is a member of the P4-ATPase subfamily and contributes to CsA and FK506 resistance

CsA is toxic to a number of filamentous fungi, however, some fungi, including the insect pathogen, *B. bassiana*, possesses intrinsic resistance to CsA (Dreyfuss et al., 1976; Traber and Dreyfuss, 1996; Zhou et al., 2016; *Figure 1-figure supplement 1A*). Although structurally different from CsA, the secondary metabolite, FK506, produced by *S. tsukubaensis*, also displays antifungal activity. Likewise, *B. bassiana* shows resistance to the drug (*Figure 1-figure supplement 1B*).

To uncover the underlying mechanism of the CsA resistance in *B. bassiana*, a random T-DNA insertion mutagenesis library was screened for sensitivity to CsA. From a screen of ~20, 000 mutant colonies, two CsA-sensitive mutants, named *mu*1 and *mu*2 were isolated (*Figure 1-Figure supplement 1C,D*). Mapping of the T-DNA insertion sites by Y-shaped adapter-dependent extension (YADE) revealed that both mutants had insertions in the same gene, but at different positions (*Figure 1A, Figure 1- figure supplement 1E*). The mutant *mu*1 contained an insertion in the coding region (at 3104 bp from the translation start site), whereas the insertion site in *mu*2 occurred in the upstream promoter sequences (at -420 bp) (*Figure 1A*). Bioinformatic analyses of the open reading frame (ORF) indicated that it encoded for a predicted protein with 1359 amino acids. Cluster analysis indicated that the protein belongs to the Type IV

P-type ATPase subfamily (P4-ATPases) (*Figure 1-figure supplement 1F,G*). The predicted topological model showed that the protein contains an A-domain (actuator domain), a N-domain (nucleotide binding domain), a P-domain (phosphorylation domain) and ten predicted transmembrane-spanning segments, which a typical P-type ATPase has (*Figure 1-figure supplement 1H*). Thus the protein was named as BbCrpa (cyclosporine A resistance P4-ATPase). In order to recapitulate the phenotype, a targeted *BbCRPA* gene-knockout strain was constructed as detailed in the methods section (*Figure 1-figure supplement 2A-C*). The Δ*BbCRPA* strain was sensitive to CsA, and the CsA-resistance defect could be complemented by the ectopic expression of *BbCRPA* in the Δ*BbCRPA* background (*Figure 1B,C*). The Δ*BbCRPA* strain also became sensitive to FK506, and the FK506-resistance defect could be complemented by the ectopic expression of *BbCRPA* in the Δ*BbCRPA* background too (*Figure 1-figure supplement 2D,E*). The Δ*BbCRPA* strain showed an approximate 4.73 ± 0.04% reduction in growth on CZP medium and a decrease in virulence using *Galleria mellonella* larvae as the target host in topical insect bioassays: LT_{50} values for the wild-type = 93.13 ± 2.49 h and Δ*BbCRPA* = 103.59 ± 1.28 h (*Figure 1-figure supplement 2F-G,J*). However, the mutation had no significant impact on sporulation (*Figure 1-figure supplement 2H,I*). To further confirm the function of BbCrpa in CsA resistance, we expressed *BbCRPA* in *V. dahliae* (the naturally CsA sensitive fungus compared to *B. bassiana*). The ectopic expression of *BbCRPA* in *V. dahliae* significantly increased fungal resistance to CsA (*Figure 1D*).

The phosphorylation of aspartic acid (D) 614 in the identified conserved P-domain DKTG sequence is crucial for ATPase activity of P-type ATPases (Palmgren and Nissen, 2011). In order to examine whether ATPase activity was required for the phenotype of CsA resistance, aspartic acid (D) 614 was replaced with arginine (R).

The D614R mutant was no longer able to confer resistance to CsA (*Figure 1-figure supplement 2K,L*). In addition, site directed mutagenesis of a conserved isoleucine (I) located in transmembrane segment M4 of P4-ATPases, to a glutamic acid (as found in Na^+/K^+ pumps) resulted in loss of ability of the protein to confer CsA resistance (Panatala et al., 2015; *Figure 1-figure supplement 2K,L*). Furthermore, although BbCrpa showed about 60% identity to Drs2p, a well-investigated P4-ATPase in *Saccharomyces cerevisiae* (NCBI Gen_locus ID: NP_009376), ectopic expression of *DRS2* in the Δ*BbCRPA* strain did not restore the resistance to CsA (*Figure 1-figure supplement 2M,N*), suggesting that BbCrpa is functionally different with Drs2p in terms of toxin resistance.

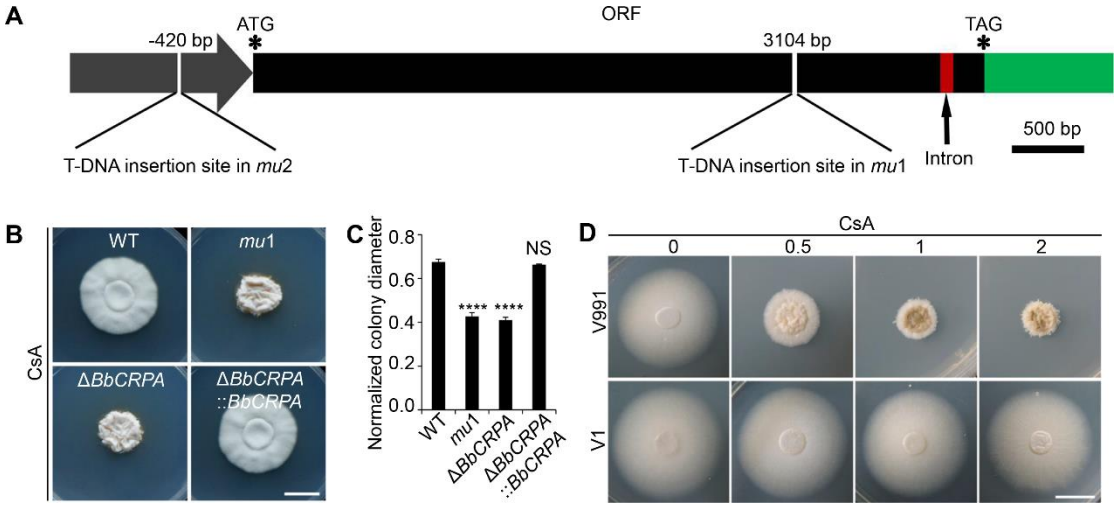

Figure 1. BbCrpa confers the resistance of *B. bassiana* and *V. dahliae* to CsA**. (A)** Schematic diagram of T-DNA insertion in *mu*1 and *mu*2. The two T-DNA insertions took place in same gene at different regions: in *mu*1, the insertion site located in the coding region (3104 bp); in *mu*2, the site was in the promoter region (-420 bp), The gene codes for a putative phospholipid-translocating P-type ATPase (P4-ATPase), named BbCrpa (cyclosporine resistance P4-ATPase) that has a 4080 bp ORF and an intron (73 bp) near its 3' end. **(B and C)** Disruption of *BbCRPA* makes *B. bassiana* sensitive to CsA. The wild-type, *mu*1, *BbCRPA* gene-knockout (Δ*BbCRPA*), and

complemented (Δ*BbCRPA*::*BbCRPA*) strains were grown on CZP + CsA (20 μg/ml). **(D)** Ectopic expression of *BbCRPA* in *V. dahliae* increases the resistance of CsA. Wild-type *V. dahliae* (V991) and V1 (expressing *BbCRPA* in *V. dahliae*) were grown on PDA and PDA + CsA (0.5 μg/ml, 1 μg/ml, and 2 μg/ml). For CsA sensitivity analysis, plates were spot inoculated with 3 μl conidial suspensions (1×10^7 conidia/ml) and incubated at 26 °C for about 10 days. The variation in growth rates was shown as [colony diameter CZP supplemented with CsA]/[colony diameter CZP]. All experiments were performed in triplicate. Data are represented as mean ± SD. ****$p < 0.0001$ from Student's *t* test. NS, not significant. Scale bars, 1 cm for (**B and D**).

The following source data and figure supplements are for figure 1:

Source data 1. Growth of target strains at CZP supplemented with CsA normalized to growth at CZP.

Figure supplement 1. *B. bassiana* shows resistance to CsA and FK506 and identification of CsA-sensitivity mutants, *mu*1 and *mu*2.

Figure supplement 2. Construction and identification of *BbCRPA* disruption strain.

CsA/FK506 is transported from TGN-EE-LE to vacuoles

As P4-ATPases have been implicated in vesicle formation and trafficking (Hua et al., 2002; Pomorski et al., 2003; Poulsen et al., 2008; Zhou and Graham, 2009), we sought to test the hypothesis that CsA/FK506 detoxification may be mediated through a P4-ATPase-mediated vesicle transport process. To this end, a dual labeling system using CsA and FK506 labeled with 5-carboxyfluorescein (the labeling did not significantly affect the toxic activity of the drugs, *Figure 2-figure supplement 1A-D*), and cells harboring red fluorescent fusion proteins of either the Rab5 or Rab7 GTPase, or the pleckstrin homology domain of the human oxysterol binding protein (PH^{OSBP})

were used. The mRFP::PH^{OSBP}, mRFP::Rab5, and mRFP::Rab7 fluorescent proteins were used as markers to visualize the *trans*-Golgi network (TGN), early endosomes (EEs), and late endosomes (LEs), respectively (Molinari et al., 1997; Pantazopoulou and Peñalva, 2009; Sugimoto et al., 2001). In separate experiments, cells treated with CsA-5-FAM or FK506-5-FAM were co-stained with the membrane-binding fluorescent dye FM4-64 used to label vesicles/vacuoles (Lewis et al., 2009). CsA-5-FAM treated wild-type cells showed membrane staining and subsequent accumulation of labeled compound in vesicles (*Figure 2A*) and vacuoles (*Figure 2B,G*), as identified by the FM4-64 co-staining. In contrast to the wild-type cell, almost no CsA-5-FAM signal could be seen inside vacuoles of the Δ*BbCRPA* mutant (*Figure 2C,G*). In the wild-type cells, CsA-5-FAM also co-localized to mRFP::PH^{OSBP} labeled *trans*-Golgi regions, as well as mRFP::Rab5 and mRFP::Rab7 labeled endosomes (*Figure 2D-F*). Similarly, FK506-5-FAM was seen in vacuoles, *via* *trans*-Golgi/endosome localizations (*Figure 2H-M*).

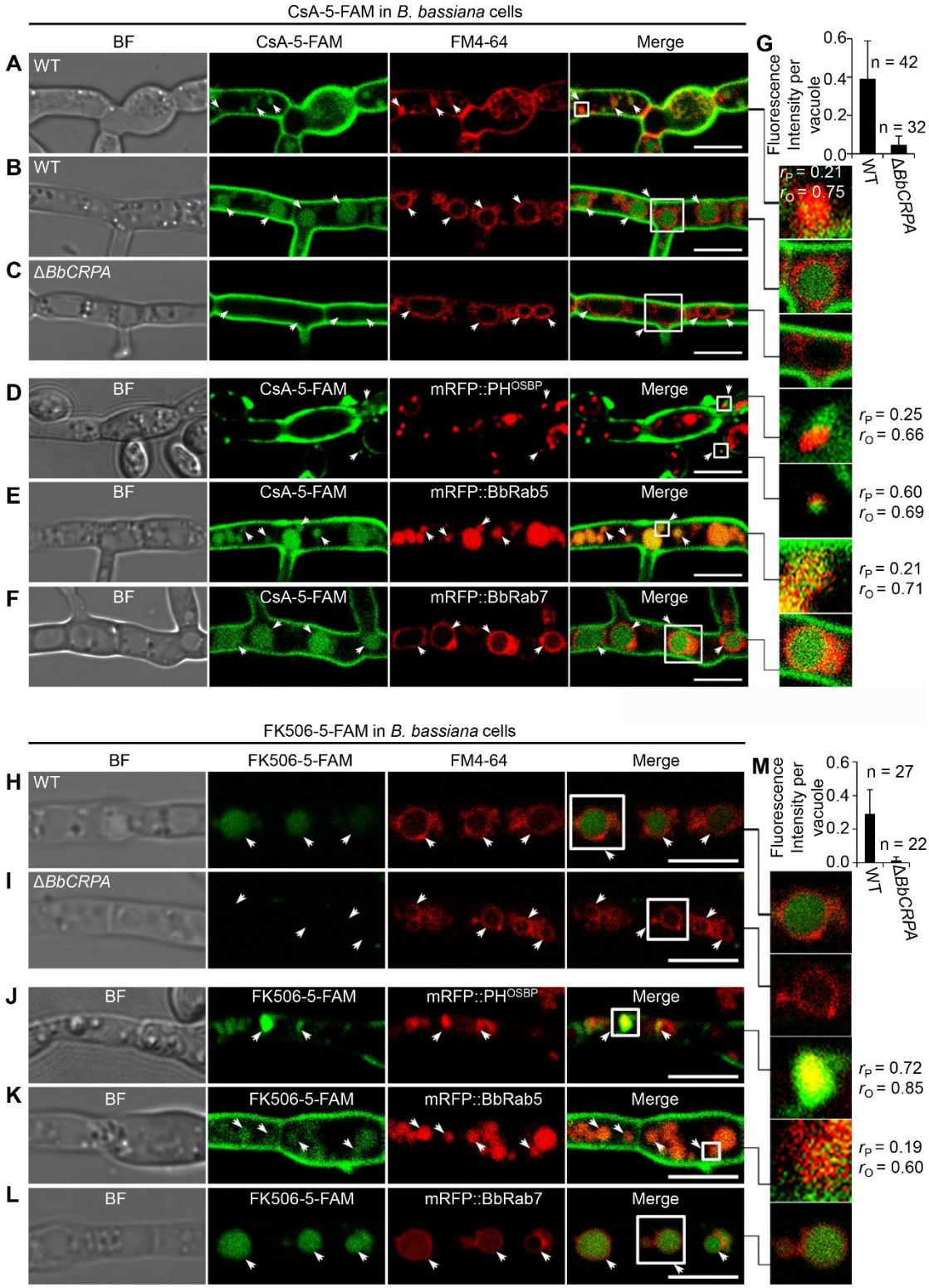

Figure 2. Distribution of fluorescein-labeled CsA and FK506 in the wild-type and Δ*BbCRPA* cells. **(A-G)** Distribution of fluorescein-labeled CsA. In the wild-type cells, fluorescein-labeled CsA (CsA-5-FAM) appeared in vesicles/endosomes (EEs) (arrows, stained by FM4-64) (**A**), TGN (arrows, marked by mRFP::PH^{OSBP}) (**D**), early

endosomes (EEs, arrows, marked by mRFP::BbRab5) (**E**), and late endosomes (LEs, arrows, marked by mRFP::BbRab7) (**F**), and accumulated in vacuoles (arrows, stained by FM4-64) (**B**); while in Δ*BbCRPA* cells, the fluorescein signal is nearly undetectable in the vacuoles (arrows) (**C**). The fluorescent intensity within the wild-type (**B**) and Δ*BbCRPA* (**C**) cells was measured by ImageJ (**G**). **(H-M)** Distribution of fluorescein-labeled FK506. In the wild-type cells, FK506-5-FAM appeared in TGN (**J**, arrows), EEs (**K**, arrows), and LEs (**L**, arrows), and accumulated in vacuoles (**H**, arrows); while in Δ*BbCRPA* cells, the fluorescein signal was nearly undetectable in the vacuoles (**I**, arrows). The fluorescent intensity within the wide-type and Δ*BbCRPA* cells was measured by ImageJ (**M**). The value of Pearson (r_P) and Overlap (r_O) correlation coefficient shows the extent of colocalization between the two target molecules. The values range between +1 (positive correlation) and -1 (negative correlation). Data are represented as mean ± SD. Scale bars, 5 μm for (**A-F, H-L**).

The following source data and figure supplement are for figure 2:

Source data 1. CsA-5-FAM/FK506-5-FAM fluorescent intensity within the wild-type and Δ*BbCRPA* cells.

Figure supplement 1. Fluorescent-labeled CsA and FK506 maintain their toxic activity.

BbCrpa acts as a component involved in vesicle trafficking through the *trans*-Golgi-endosomes to vacuoles

A series of ten different eGFP-BbCrpa fusion proteins were constructed to observe the subcellular localization of BbCrpa. By testing for complementation of the Δ*BbCRPA* phenotype, BbCrpa bearing eGFP at the N- or C-terminus, or at the regions between transmembrane segments 4-5, 8-9, and 9-10, remained capable of mediating CsA

238 detoxification (*Figure 3-figure supplement 1A-G*). The eGFP-BbCrpa N-terminal
239 fusion protein (eGFP::BbCrpa) was used for further study. In conjunction with
240 FM4-64 staining, fluorescent signal derived from eGFP::BbCrpa could be seen in the
241 apical plasma membrane and cytosolic structures in germinating conidia and the eGFP
242 signal also emerged in the subapical region called the Spitzenkörper in germ tubes
243 (*Figure 3-figure supplement 1H,I*). In hypha, dual labeling with eGFP::BbCrpa and
244 mRFP::PH^{OSBP} revealed the co-localization of both signals in *trans*-Golgi (*Figure 3A*),
245 with continued co-localization at discrete spots as well as accumulation of the eGFP
246 signal in vacuoles (*Figure 3B*). A similar pattern could be seen with co-staining
247 experiments using FM4-64, which also allowed for staining of the vesicle/vacuole
248 membranes containing the eGFP::BbCrpa signal (*Figure 3C*). Dual labeling with
249 eGFP::BbCrpa and mRFP::BbRab5 (*Figure 3D*), and eGFP::BbCrpa and
250 mRFP::BbRab7 (*Figure 3E*) revealed the localization of BbCrpa in EEs and LEs,
251 respectively. eGFP::BbCrpa and FM4-64 staining showed the localization of BbCrpa
252 in vesicles (*Figure 3C*) or vacuoles (*Figure 3F*). FM1-43 is another membrane probe
253 that has been widely used for monitoring recycling of vesicles (Hansen et al., 2009).
254 The staining of FM1-43 revealed that both mRFP::BbRab5 and mRFP::BbRab7 were
255 co-localized with FM1-43 (*Figure 3-figure supplement 1J,K*), and BbCrpa exhibited
256 vesicular and vacuolar localization (*Figure 3-figure supplement 1L*). Feeding
257 5-FAM-labeled CsA or FK506 to cells expressing an mRFP tagged version of BbCrpa
258 (mRFP::BbCrpa), the two signals were colocalized in some puncta on the plasma
259 membrane, and the signals were ultimately converged in vacuoles (*Figure 3G-J*).
260 Time-lapse dual-label microscopy combining either eGFP::BbCrpa and FM4-64 or
261 eGFP::BbCrpa and mRFP::PH^{OSBP} indicated the dynamic trafficking through the
262 described pathway from the vesicles to early/late endosome, and to vacuoles (*Figure*

263 *3K-L, Supplementary files 1,2*). Whereas the eGFP::BbCrpa and FM4-64 staining
264 showing vacuolar localization of the *B. bassiana* P4-ATPase (*Figure 3F*), the
265 heterologous expression of an eGFP-tagged version of the yeast homolog,
266 eGFP::Drs2p, showed cytoplasmic localization of this protein (*Figure 3M*).

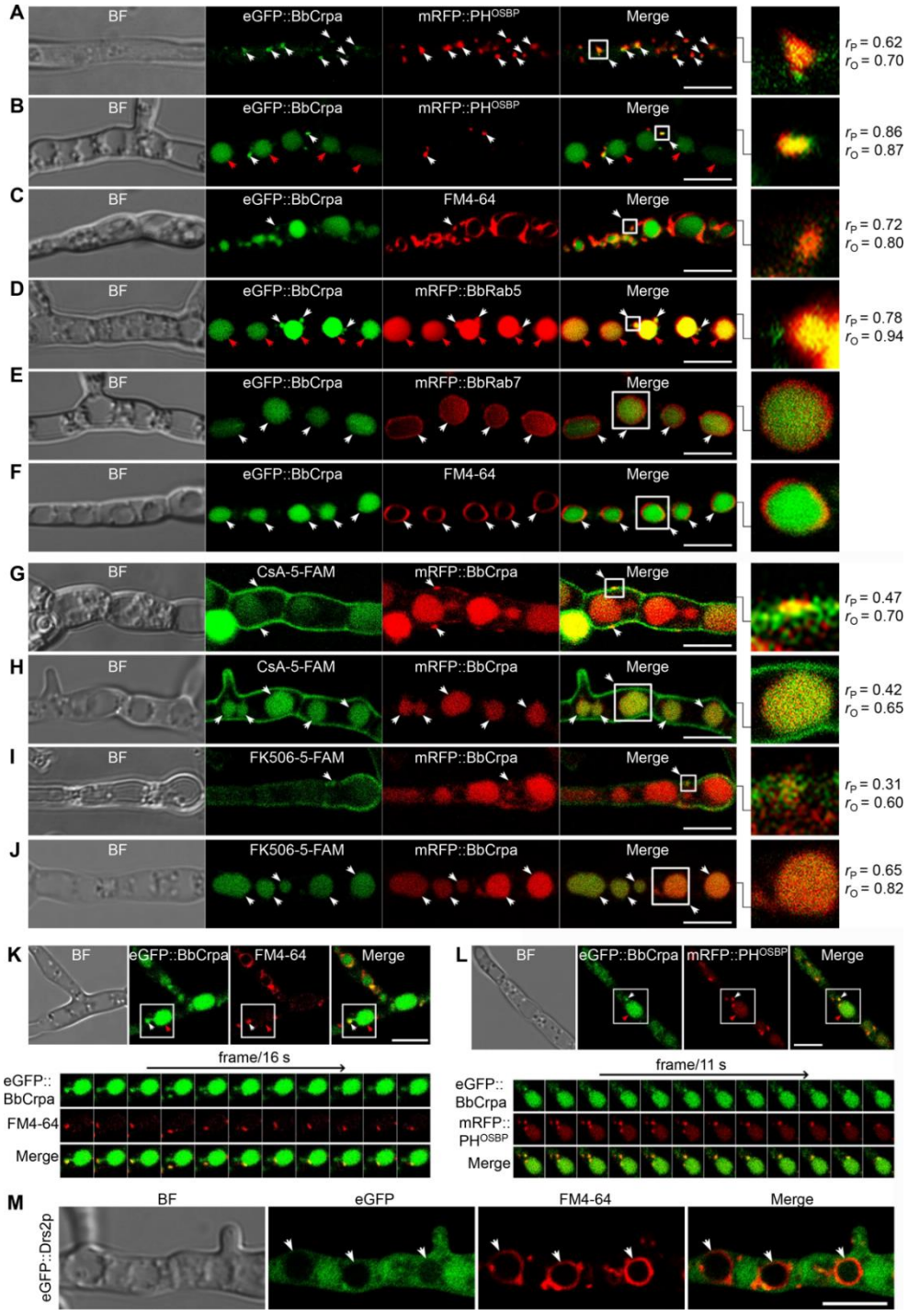

267 **Figure 3.** Subcellular localization and dynamic trafficking of BbCrpa. **(A and B)**

eGFP::BbCrpa colocalizes with mRFP::PH^{OSBP} at TGN (white arrows) and accumulates in vacuoles (red arrows, see also that in (**F**, white arrows)). **(C)** eGFP::BbCrpa accumulates in vesicle (arrows) that is stained by FM4-64. **(D)** eGFP::BbCrpa colocalizes with mRFP::BbRab5 in early endosomes (EEs, white arrows) and then accumulates in vacuoles (red arrow, also see in (f, white arrows)). **(E)** eGFP::BbCrpa colocalizes with mRFP::BbRab7 in late endosomes (LEs, arrows). **(F)** eGFP::BbCrpa accumulates in mature vacuoles (arrows) which are stained by FM4-64. **(G)** mRFP::BbCrpa colocalizes with CsA-5-FAM in puncta on the plasma membrane (arrows). **(H)** mRFP::BbCrpa colocalizes with CsA-5-FAM in vacuoles (arrows). **(I)** mRFP::BbCrpa colocalizes with FK506-5-FAM in puncta on the plasma membrane (arrows). **(J)** mRFP::BbCrpa colocalizes with FK506-5-FAM in vacuoles (arrows). **(K)** eGFP::BbCrpa appears in vesicles (white arrows) and moves into vacuoles (red arrows). Time to acquire one image pair was 16 s. **(L)** eGFP::BbCrpa colocalizes with vesicle from TGN which was labeled by mRFP::PH^{OSBP} (white arrows) and transports into vacuole (red arrows). Time to acquire one image pair was 11 s. **(M)** Localization of eGFP::Drs2p in *B. bassiana* cells. eGFP::Drs2p does not accumulate in vacuoles (arrows) which were stained by FM4-64. Scale bars, 5 μm for (**A-M**). The value of Pearson (r_P) and Overlap (r_O) correlation coefficient shows the extent of colocalization between the two target molecules. The values range between +1 (positive correlation) and -1 (negative correlation).

The following figure supplement and supplementary files are for figure 3:

Figure supplement 1. BbCrpa N-terminally tagged with eGFP maintains its original function and is localized to the apical plasma membrane and Spitzenkörper of *B. bassiana*.

Supplementary file 1. Time-lapse imaging of the trajectory of eGFP::BbCrpa (green)

and vesicle (red) labeled by FM4-64. Time to acquire one image pair was 1 s. Scale bar, 5 µm.

Supplementary file 2. Time-lapse imaging of the trajectory of eGFP::BbCrpa (green) and vesicle (red) derived from TGN which was labeled by mRFP::PH^{OSBP} (red). Time to acquire one image pair was 1 s. Scale bar, 5 µm.

Contributions of BbCrpa N- and C-terminal tails to CsA/FK506 detoxification

BbCrpa has a 268 amino acid cytosolic N-terminal tail before the first transmembrane segment and an 86 amino acid cytosolic C-terminal tail after the last membrane segment (*Figure 1-figure supplement 1H*). Deletion of either the N- (1-268 aa) or the C-terminus (1274-1359 aa) eliminated the detoxification activity of BbCrpa (*Figure 4A-C, Figure 4-figure supplement 1A-B*). Microscopic visualization of N-terminal eGFP fusion constructs to the N- and C-terminal deletion mutants (eGFP::dB^N and eGFP::dB^C) revealed that loss of the N terminus (eGFP::dB^N) eliminated vacuolar localization of the protein, whereas the eGFP::dB^C protein was still able to traffic to vacuoles (*Figure 4-figure supplement 1E*).

In order to further probe the contributions of the N- and C-terminal domains of BbCrpa in mediating CsA/FK506 detoxification, we substituted the homologous N- and C-terminal domains of the yeast Drs2p (that does not complement the CsA/FK506 susceptibility phenotype of the *BbCRPA* mutant strain) (*Figure 4A*). The resulting chimeric proteins with either C-terminus or N-terminus from BbCrpa alone unable to restore CsA-/FK506-tolerance to the cell (*Figure 4D-E, Figure 4-figure supplement 1C-D*). However, the simultaneous substitution of the BbCrpa N- and C-terminal domains into the yeast protein led to a chimera that showed a significant increase in resistance to CsA/FK506 compared to the natural Drs2p (*Figure 4D-E, Figure 4-figure supplement 1C-D*).

To identify the key motif (s) in the N-terminus responsible for vacuolar targeting, a series of N-terminal deletion mutants fused with mRFP were generated. These included: (1) B^{N1-268}::mRFP, (2) $B^{N151-268}$::mRFP, (3) $B^{N216-268}$::mRFP, (4) $B^{N226-268}$::mRFP, (5) $B^{N236-268}$::mRFP, (6) $B^{N246-268}$::mRFP, (7) $B^{N256-268}$::mRFP, (8) $B^{N257-268}$::mRFP, (9) $B^{N258-268}$::mRFP, (10) $B^{N259-268}$::mRFP (*Figure 4F, Figure 4-figure supplement 1F*). All the mutants retained the wild-type vacuolar localization except $B^{N259-268}$::mRFP (*Figure 4F, Figure 4-figure supplement 1F*). These data indicated that the N-terminal sequence, F^{258}ASFLPKFLFE^{268}, is critical for vacuolar targeting of BbCrpa. The amino acid residue, K (lysine) was identified as a putative mono-ubiquitination site (Baxter et al., 2005; MacGurn et al., 2012). In order to probe whether K264 residue was required for vacuolar targeting, a site directed mutant, F^{258}ASFLPAFLFE^{268} (K264A), was generated. Microscopic visualization revealed that K264 function as a critical residue for proper targeting of $B^{N258-268\ (K264A)}$::mRFP (*Figure 4F)*. Western blot analysis further showed that K264 is responsible for the ubiquitination of $B^{N258-268\ (K264A)}$::mRFP (*Figure 4-figure supplement 1G*).

A C-terminal deletion mutant, $\Delta B^{C1326-1359}$ (deletion of 1326-1359 aa of BbCrpa), did not affect CsA/FK506 resistance (*Figure 4A-C, Figure 4-figure supplement 1A,B*). However, removal of one additional amino acid, Y1325 (tyrosine), resulting in the mutated protein, $\Delta B^{C1325-1359}$, led to a significant decrease in resistance to CsA/FK506 (*Figure 4A-C, Figure 4-figure supplement 1A,B*). For further investigation of this tyrosine function, we conducted site directed mutagenesis of Y1325 to A (alanine). The mutation led to a significant decrease in CsA/FK506 resistance (*Figure 4A-C, Figure 4-figure supplement 1A,B*). Sequence analysis indicated the presence of two additional nearby (in the C-terminus) tyrosine residues: Y1341 and Y1350 (*Figure 4A)*. Site directed mutants bearing double substitution mutations of (1)

343 Y1325A-Y1341A, and (2) Y1325A-Y1350A, and a triple substitution mutation: (3)
344 Y1325A-Y1341A-Y1350A resulted in significant decreases in CsA/FK506 resistance
345 as compared to the wild-type protein and as compared to the Y1325A single mutant
346 (*Figure 4A-C, Figure 4-figure supplement 1A,B*). These results suggest a key role of
347 these tyrosine residues, in particular, Y1325, for the detoxification activity of BbCrpa.

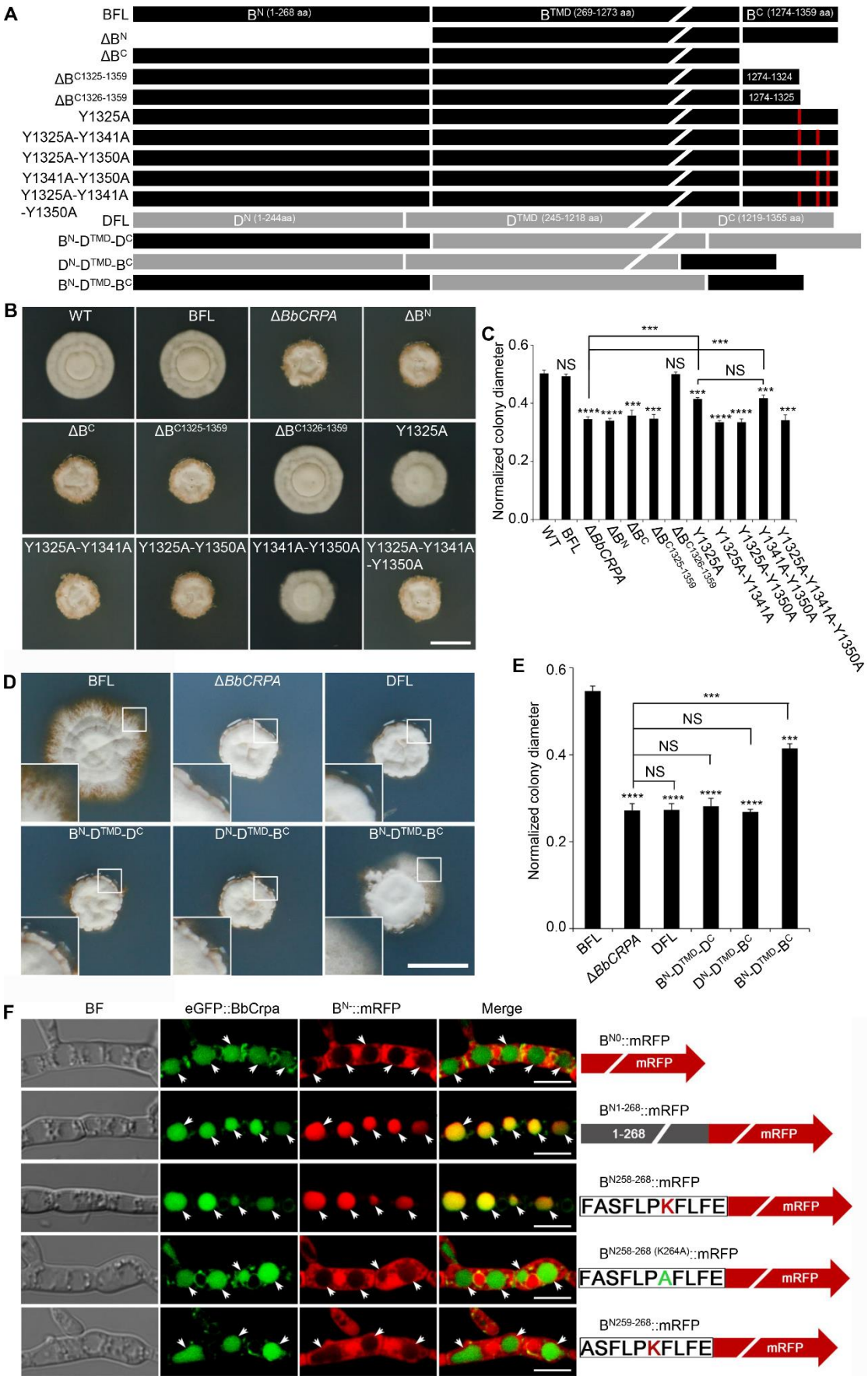

348 **Figure 4.** Y1325 (Tyr) in C-terminus is critical for detoxification, and the N-terminus

is essential for vacuolar targeting. **(A)** Schematic model of N- and C-terminal deletion of BbCrpa and the graft of the N- and C-terminus of BbCrpa with Drs2p. BFL, BbCrpa full length; B^{N}, BbCrpa N-terminus; B^{TMD}, BbCrpa transmembrane-domain; B^{C}, BbCrpa C-terminus; DFL, Drs2p full length; D^{N}, Drs2p N-terminus; D^{TMD}, Drs2p transmembrane-domain; D^{C}, Drs2p C-terminus. **(B and C)** BbCrpa C-terminus Y1325 is critical for the detoxification of CsA. All strains were incubated in CZP + CsA (20 μg/ml). **(D and E)** BbCrpa N- and C-terminus are crucial for Drs2p detoxification activity. All strains were incubated in CZA + CsA (20 μg/ml). **(F)** The last 11 amino acid residues of BbCrpa N-terminus contains vacuolar localization signal. BbCrpa N-terminus ($B^{N1\text{-}268}$, $B^{N258\text{-}268}$) fused with mRFP are obviously colocalized with BbCrpa in vacuoles. When the K264 (Lys) was replaced by Ala (**A**), the guiding function was disappeared. $B^{N\text{-}}$::mRFP, mRFP fused with different length of N-terminus of BbCrpa. For CsA sensitivity analysis, plates were spot inoculated with 3 μl conidial suspensions (1×10^{7} conidia/ml) and incubated at 26 ºC for about 10 (CZP/CZP + CsA) or 14 (CZA/CZA + CsA) days. The variation in growth rates was shown as [colony diameter CZP/CZA supplemented with CsA]/[colony diameter CZP/CZA]. All experiments were performed in triplicate. Data are represented as mean ± SD. ***p < 0.001; ****p < 0.0001 from Student's *t* test. NS, not significant. Scale bars, 1 cm for (**B and D**) and 5 μm for (**F**).

The following source data and figure supplement are for figure 4:

Source data 1. Growth of target strains at CZP/CZA supplemented with CsA normalized to growth at CZP/CZA.

Figure supplement 1. Y1325 (Tyr) in C-terminus is critical for detoxification of FK506 and the N-terminus is essential for vacuolar targeting.

Exogenous overexpression of *BbCRPA* in *A. thaliana* and *G. hirsutum* increases

the resistance to Verticillium wilt disease

The phyotopathogenic fungus, *V. dahliae Kleb* is responsible for causing a devastating wilt disease infecting many important trees and crops including elm, cotton, potato, pepper, watermelon, mint, and lettuce (Subbarao et al., 1995; Veronese et al., 2003). Toxins (*V. dahliae* toxins, VD-toxins) produced by the fungus contribute to wilt symptoms (Fradin and Thomma, 2006; Keen et al., 1972; Meyer et al., 1994). Cinnamyl acetate (CIA) is one of the major lipophilic VD-toxins identified (Laouane et al., 2011). Detoxification of such mycotoxins might represent an effective way to decrease the damage causing by phytopathogens (Wang et al., 2020). Expression of *BbCRPA* in *V. dahliae* significantly increased the resistance of the fungus to CsA (*Figure 1D*). The cross-species resistance endowed by BbCrpa to the toxin promotes us to test whether BbCrpa could be broadly exploited for detoxification of the fungal mycotoxin CIA in plants. To this end, we generated transgenic *A. thaliana* and *G. hirsutum* in which *BbCRPA* was under control of a constitutive promoter CaMV35S. Southern blot results validated *BbCRPA* insertion in Arabidopsis and cotton, and qRT-PCR confirmed the transcription of the gene in transgenic plants (*Figure 5-figure supplement 1A-F*). The expression of *BbCRPA* in *A. thaliana* increased resistance to CIA (*Figure 5A*). With little or no growth was seen in control plants in the presence of 50 μg/ml CIA, under the condition in which plants expressing *BbCRPA* were able to grow (*Figure 5A*). Plant bioassays, infecting either *A. thaliana* or *G. hirsutum* with *V. dahliae*, revealed a significant reduction in symptom severity (*Figure 5B-G*). In order to probe the potential mechanism mediating the detoxification

of CIA, FITC labeled CIA was fed to plants with sections counterstained with FM4-64 (*Figure 5H,I*). These data showed the promoted accumulation of CIA in vacuoles in *BbCRPA* transformed plant cells, and not in the wild-type parent.

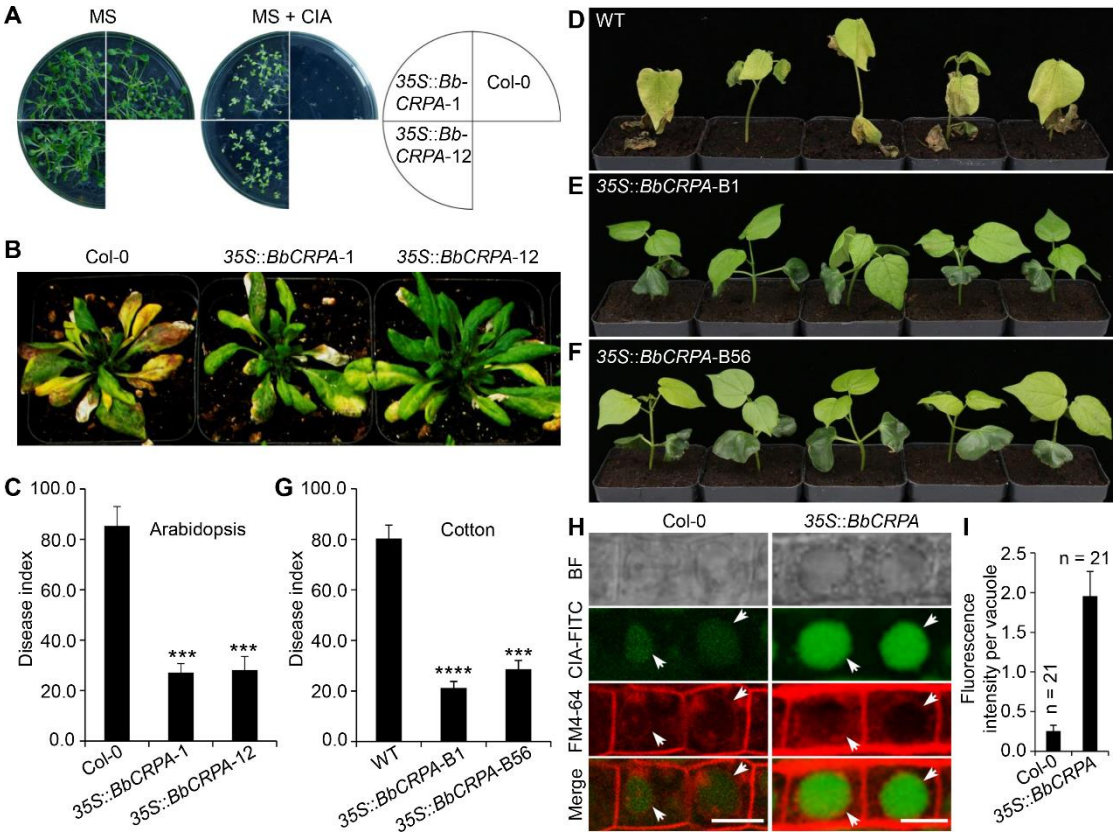

Figure 5. Exogenous overexpression of *BbCRPA* in Arabidopsis and cotton increases the resistance to *V. dahliae*. **(A)** Exogenous overexpression of *BbCRPA* increases the resistance of Arabidopsis to CIA. The wild-type (Columbia, Col-0) and *35S::BbCRPA* seedlings were grown for 14 days on MS medium containing either 0.5% DMSO (control) or 50 μg/ml CIA. **(B and C)** Exogenous overexpression of *BbCRPA* increases the resistance of Arabidopsis to *V. dahliae.* Each Arabidopsis plant (4-5 leaves) was inoculated with 3 ml *V. dahliae* spore suspension (2×10^8 spores/ml), and the disease index of T_3 transgenic plants and the wild-type plants to *V. dahliae* was evaluated 21 days after inoculation. **(D-G)** Exogenous overexpression of *BbCRPA* in cotton increases the resistance to *V. dahliae*. 10-day-old cotton seedling roots were

infected by *V. dahliae* spore suspension (1×10^7 spores/ml), and the disease index of T2 transgenic cottons to *V. dahliae* was evaluated 14 days after inoculation. **(H and I)** Exogenous overexpression of *BbCRPA* in Arabidopsis promotes the accumulation of cinnamyl acetate (CIA) in vacuoles of root cells. Strong fluorescein-labeled CIA (CIA-FITC) signal was observed in vacuoles of transgenic Arabidopsis cells (*35S*::*BbCRPA*), while only very weak signal was observed in the vacuoles of wild-type Arabidopsis cells (arrows) (**H**). Vacuoles (arrows) were indicated by FM4-64 and plants were treated with 5 μg/ml CIA-FITC. The comparison of fluorescent intensity in vacuoles between the wild-type and *35S::BbCRPA* transgenic Arabidopsis was measured by ImageJ (**I**). Scale bars, 10 μm. The resistance of plants to *V. dahliae* was estimated by disease index (DI). Data are representative of three independent experiments with at least 15 plants per replication for Arabidopsis, and 30 plants per replication for cotton. Data are represented as mean ± SD. ***$p < 0.001$; ****$p < 0.0001$ from Student's *t* test.

The following source data and figure supplement are for figure 5:

Source data 1. Disease index and fluorescent intensity.

Figure supplement 1. Validation of transgenic *BbCRPA* plants.

Discussion

Mounting reports have documented that P4-ATPases display important roles in vesicle biogenesis, membrane trafficking or remodeling, signal transduction, biotic-/abiotic-stress response, and polarized growth. Nevertheless, little is known about their function in cell detoxification. In the present study, we identify a P4-ATPase gene, *BbCRPA*, from insect disease fungus *B. bassiana* that displays resistance to CsA and FK506. The colocalization of CsA/FK506 and BbCrpa to the puncta on plasma membrane (*Figure 3G,I*) suggests that the toxins are wrapped into

vesicles there. Then, the toxins are delivered into vacuoles for compartmentation, which confers the resistance of CsA and FK506 to the fungus.

In eukaryotic cells, another catabolic pathway that sequesters undesired materials is autophagy (Kaufmann et al., 2014). In autophagy pathway, the membrane of autophagosome is newly formed (Barz et al., 2020). In P4-ATPases-mediated vesicle formation, however, the membrane of the vesicle is from where the P4-ATPase is located on. The P4-ATPases catalyze the translocation of phospholipids from the exoplasmic to the cytosolic membrane leaflet to establish phospholipid asymmetry in biological membranes, and thus to promote budding of transport vesicles. Knocked out *ATG1*, a crucial factor for regulating of autophagosome-vacuole fusion, we found the disruption does not affect the resistance to CsA, as well as the formation of autophagosome in *B. bassiana* (*Supplementary file 3A-C*), suggesting that BbCrpa-mediated detoxification is independent of autophagy pathway.

B. bassiana can be dormant in soil for years. As a pathogen, the fungus can infect insects; as an endophyte, it can reside in plants., it can reside in plants (Ownley, et al., 2008; Xiao, et al., 2012). To survive, *B. bassiana* evolves mechanisms to protect it from harmful materials produced by microorganisms, insects, or plants. CsA is a secondary metabolite produced by *B. nivea,* another entomopathogenic fungus of *Beauveria* (Margaritis and Chahal, 1989). This small lipophilic polypeptide can freely cross the plasma membrane (Hunt and Morshead, 2010). The lipophilic macrolide FK506 is produced by the soil borne streptomycete, *S. tsukubaensis* (Barreiro et al., 2012). Both CsA and FK506 bind to their cognate immunophilins, Cyps and FKBPs, to form binary complexes which then block the phosphatase activity of calcineurin, or inhibit the peptidyl-prolyl *cis-trans* isomerase (PPIase) activity of Cyps and FKBPs

and thus impair Cyps-/FKBPs-mediated protein folding (Kang et al., 2008; Wang and Heitman, 2005). Interestingly, although *B. bassiana* and *B. nivea* belong to same genus, no cyclosporin synthetase genes was found in *B. bassiana* genome (https://fungismash.secondarymetabolites.org/#!/start), while no BbCrpa homologue was detected in *B. nivea* (https://blast.ncbi.nlm.nih.gov/Blast.cgi). Therefore, it is acceptable that for competition and survival, *B. bassiana* has developed a unique vesicle-mediated detoxification mechanism against CsA; while *B. nivea*, the toxin producer, has its own orchestrated delivery and timing system, as well as subcellular containment system, to avoid self-harm from the toxin (Keller, 2015).

Although the closest homologue among five yeast P4-ATPases to BbCrpa is Drs2p, functions of BbCrpa are quite different from those of Drs2p. Strong BbCrpa signal was observed in vacuoles, but no Drs2p signal was detected in the vacuoles (*Figure 3F,M*). It has been known that Drs2p is required for AP-1/Clathrin-coated vesicle formation (Liu et al., 2008). However, BbCrpa-mediated resistance to CsA is independent with AP-1 and Clathrin (*Supplementary file 3D,E*). NPFXD motifs can interact with the Sla1p homology domain 1 (SHD1) of Sla1p that serves as the targeting signal recognition factor for $NPFX_{(1,2)}D$-mediated endocytosis (Howard et al., 2002; Liu et al., 2007). Drs2p has two NPFXD motifs in its C-terminal tail. In contrast, no NPFXD motif is found in the C-terminus of BbCrpa, suggesting that this P4-ATPase may be not involved in NPFXD/Sla1p endocytosis pathway. In addition, our N-terminal serial deletion and mRFP tagging results reveal that the last eleven-amino acid residues (F^{258}ASFLPKFLFE^{268}) are capable of guiding protein into the vacuole (*Figure 4F*). When the Lys residue was replaced by Ala, the residues loses the vacuole-target function, implying that the process is associated with ubiquitination modification (*Figure 4F, Figure 4-figure supplement 1G*). For Drs2p, no

FASFLPKFLFE homologous sequence is present in its N-terminal tail, supporting the previous studies that Drs2p-mediated vesicle transport pathway is between TGN and EE or plasma membrane and TGN, but not including the journey to the vacuole (Liu et al., 2007). In N-terminal tail of Drs2p there are two potential PEST motifs and one poor PEST motif (Liu et al., 2007). PEST motif is considered as a signature of proteins that would be degraded through the ubiquitin pathway (Roth et al., 1998). However, no typical PEST motif was found in BbCrpa N-terminus. This suggests that Drs2p is the target for ubiquitin-mediated degradation in proteasome while BbCrpa may be involved in the turnover of the membrane protein in TGN membrane or vacuole membrane (Ciechanover, 1998; Rotin et al., 2000). Most importantly, BbCrpa can confer resistance of CsA/FK506 to the cell while Drs2p cannot (*Figure 4A,D-E, Figure 4-figure supplement 1C,D*).

Protein tyrosine phosphorylation/dephosphorylation is an important mechanism for regulating of many cellular processes (Ghelis, 2011; Rosenblum et al., 1995; Schlessinger and Ullrich, 1992). It was reported that CsA/Cyps and FK506/FKBP12 participated in the regulation of protein tyrosine phosphorylation/dephosphorylation (Bauer et al., 2009; Lopez-Ilasaca et al., 1998). For example, interleukin-2 tyrosine kinase (Itk) is a protein tyrosine kinase of the Tec family. The tyrosine kinase activity of Itk is inhibited by CypA *via* forming a stable complex, and CsA can increase the phosphorylation levels of Itk thus relieving the inhibition of CypA on it (Brazin et al., 2002). We show a possible role of Y1325 phosphorylation in detoxification activity of BbCrpa (*Figure 4A-C*). The common target of CsA/Cyp and FK506/FKBP12 is calcineurin, also a PP2B enzyme. Typically, calcineurin is a serine/threonine protein phosphatase. Although it had been reported that calcineurin can also dephosphorylate phosphotyrosine containing proteins (Carrera et al., 1996; Chan et al., 1986; Faure et

al., 2007), no PXIXIT nor LXVP motif, the binding motifs of calcineurin (Shi, 2009), was found in BbCrpa sequence, suggesting that the phosphorylation/dephosphorylation of Y1325 may not be regulated directly by calcineurin. Does (or how does) CsA/FK506 stimulate the tyrosine phosphorylation of BbCrpa awaits further investigation.

Toxins produced by pathogens are recognized as a pathogenic factor in many plant diseases (Tsuge *et al*, 2013). For plant disease control, cell detoxification strategy can prevent plants from the toxicity, thus ensuring hosts exhibit their innate immunity against the pathogens (Wang et al., 2020). In this study, the ectopic expression of *BbCRPA* in *V. dahliae* significantly increases the resistance of the fungus against CsA, demonstrating that this P4-ATPase can display its detoxification ability in other species. We then exogenously overexpressed the gene in cotton and Arabidopsis. The transgenic plants exhibit significantly increased resistance to the Verticillium wilt disease (*Figure 5A-G*). Meanwhile, the vacuole-targeted transport of the toxic material (i.e., cinnamyl acetate, CIA) produced by the wilt-disease fungus *V. dahliae* was significantly promoted, indicating that CIA is also the cargo of BbCrpa-mediated vesicle transport in plant cells. Details about what properties the compounds should have and how the P4-ATPases recognize their cargoes await further investigations. Nevertheless, the method described here allows us to identify other P4-ATPases that are able to detoxify various mycotoxins, such as voitoxin, trichothecenes, fumonisins, and ochratoxin A, which are not only involved in the virulence of the phytopathogenic fungi but also extremely harmful for human and animal health.

The P4-ATPase-conferred resistance to CsA/FK506 also suggests a strategy through the vesicle transport associated detoxification to reduce the side effects of the drugs in human organ transplant operation and autoimmune-diseases therapy. Besides,

using the fluorescein-labeled compounds and proteins as probes allows us to observe the real time process of cargo delivering as well as dynamic alteration of vesicles, EEs, LEs, and vacuoles *in vivo*, thus providing a simple and effective platform to study the subcellular processes of P4-ATPase mediated vesicle transport and the important aspects of the compartmental detoxification in living cells.

In conclusion, our study reveals the molecular mechanism of the intrinsic resistance possessed by *B. bassiana* to the CsA and FK506, and shows a new role of P4-ATPases in cell detoxification. The cross-species resistance endowed by the P4-ATPase to toxins can be exploited for plant disease control and human health protection.

Materials and methods

Strains and culture conditions

Beauveria bassiana wild-type (CGMCC7.34, China General Microbiological Culture Collection Center, CGMCC) and mutant strains were grown on Czapek-Dox broth (CZB) or agar (CZA) (233810, BD-Difco, USA), or CZB or CZA supplemented with 0.25% (wt/vol) tryptone (CZP). *Verticillium dahliae* strain V991 (kindly gifted by Prof. Guiliang Jian) was grown on Potato Dextrose broth (PDB) or agar (PDA) (254920, BD-Difco). *Escherichia coli* DH5α (9057, Takara) and *Agrobacterium tumefaciens* AGL-1 (Lab stock) were used for routine DNA manipulations and fungal transformations, respectively. *Agrobacterium tumefaciens* GV3101 (Lab stock) and LBA4404 (Lab stock) were used for Arabidopsis (Col-0, CS60000, Arabidopsis Biological Resource) and cotton (*cv.* Jimian 14, kindly donated by Prof. Zhiying Ma) transformation, respectively.

Inhibition ring assay

Filamentous fungi used in inhibition ring assay include *Beauveria bassiana*, *Metarhizium anisopliae* (kindly gifted by Prof. Weiguo Fang), *Botrytis cinerea* (3.4584, CGMCC), *Alternaria brassicae* (3.7804, CGMCC), *Alternaria brassicicola* (3.7805, CGMCC), *Aspergillus nidulans* (3.15737, CGMCC), *Alternaria solani* (Lab stock). The fungi were inoculated into PDA medium except *Botrytis cinerea* (regeneration medium: 0.1% yeast extract, 24% sucrose) and *Aspergillus nidulans* (modified PDA medium containing 0.11% uracil and 0.12% uridine) at 26 ºC for about 10-14 days for conidia harvested. Then, for each strain, 300 μl of fungal conidial suspensions (1×10^7 conidia/ml in 0.05% Tween-80, A600562, Sangon Biotech, China) was added into 60 ml PDA (approximately 45 ºC, *A. nidulans* conidial suspension was added into the modified PDA medium) medium, mixed evenly and poured into three Petri Dishes (diameter = 90 mm), averagely. After the media completely solidified, punch four holes of 5-mm diameter equally distant apart in Petri Dishe. Each well was added with 5 μl different concentrations of CsA (B1922, APEXBIO) or FK506 (B2143, APEXBIO), and the dishes were incubated at 26 ºC for about 4-7 days.

Screening of CsA-Sensitive mutants and isolation of the target gene

B. bassiana random insertion (T-DNA) library was constructed as described previously (Fang et al., 2004). Plasmid pK2 was used as frame vector. *Bar*::*Gus* fusion reporter gene was placed into pK2 between the *A. nidulans gpdA* promoter and

576 *trpC* terminator. CZP medium containing CsA (20 μg/ml) was used to screen
577 CsA-sensitive mutants. The desired genomic sequence was isolated by PCR walking
578 using the YADE method as described previously (Fang et al., 2005).

579 **Construction of Δ*BbCRPA* and complementation strains**

580 A list of primers used in the nucleic acid manipulations was given in Supplementary
581 file 4. LA Taq (RR002A, TaKaRa) or PrimeSTAR MAX Premix (R045, TaKaRa) was
582 used for the generation of PCR products. The resultant products were cloned into
583 target vectors using T4 DNA ligase (CV0701, Aidlab).

584 The construct of *BbCRPA* gene disruption was generated by homologous
585 recombination. Plasmid pK2-*Bar* containing herbicide (phosphinothricin, P679,
586 PhytoTech) resistance gene (*Bar)* that was sandwiched between *A. nidulans trpC*
587 promoter and *trpC* terminator was used as backbone to construct the transformation
588 vector. The vector was constructed as follows: a 5' end 1.294-kb sequence (1053-2346
589 bp) and a 3' end 1.214-kb (2897-4110 bp) of *BbCRPA* were amplified by PCR (LA
590 Taq) using *B. bassiana* genomic DNA as template with primer pairs
591 *BbCRPA*LB-F/*BbCRPA*LB-R and *BbCRPA*RB-F/*BbCRPA*RB-R, respectively. The 3'
592 end PCR product flanking with *Xba*I and *Hin*dIII restriction sites was digested with
593 *Xba*I (FD0684, Thermo Scientific) and *Hin*dIII (FD0504, Thermo Scientific), and
594 then linked with *Bar* cassette to form *Bar-BbCRPA*3'. Similarly, *BbCRPA* 5' end PCR
595 product that contains *Eco*RI (FD0274, Thermo Scientific) sites was fused with
596 *Bar-BbCRPA*3' to generate pK2-*BbCRPA*5'-*Bar-BbCRPA*3'. The resulting vector was
597 transformed into *A. tumefaciens* AGL-1, which was then used to transform wild-type

598 *B. bassiana* as described previously (Fang et al., 2004). Mutant colonies were single
599 spore isolated and the correct integration event was verified by PCR using 2 × Taq
600 Master Mix (E005-2b, Novoprotein) with primers *MCS*-F/*MCS*-R and qRT-PCR with
601 primer pair *BbCRPA*ex-F/*BbCRPA*ex-F.

602 The selection marker gene, *Sur*, conferring sulfonylurea (chlorimuron-ethyl,
603 J66605, Alfa Aesar, USA) resistance was used for complementation vector
604 construction. The gene was amplified from pCB1536 with primer pair *Sur*-F/*Sur*-R
605 (Zhang et al., 2010). The PCR product was digested with *Not*I (FD0594, Thermo
606 Scientific) and *Bam*HI (FD0055, Thermo Scientific), and then inserted into modified
607 PUC-T vector (D2006, Beyotime) between *A. nidulans trpC* promoter and *A. nidulans*
608 *trpC* terminator. The vector was digested with *Eco*RI and *Hin*dIII and inserted into the
609 corresponding sites of pK2-*Bar*, replacing the *Bar* gene, to generate pK2-*Sur*. The
610 complementation vector, pK2-*Sur*-*BbCRPA*, was constructed using a 5998 bp
611 fragment that contains the entire ORF (4153 bp including a 73 bp intron), 1072 bp of
612 upstream, and 773 bp of downstream sequences. The fragment was amplified *via* PCR
613 (PrimeSTAR MAX Premix) with primers *Com*-F and *Com*-R using *B. bassiana*
614 genomic DNA as template. The PCR product was digested with *Spe*I (FD1254,
615 Thermo Scientific) and *Xba*I and then inserted into pK2-*Sur* to form
616 pK2-*Sur*-*BbCRPA*. The resulting vector was used for Δ*BbCRPA* transformation.

617 **Site-directed mutagenesis of BbCrpa and N/C-terminal tail exchange between**
618 **BbCrpa and Drs2p**

619 For the change of Ile (562) to Glu (I562E), and Asp (614) to Arg (D614R) of BbCrpa,

the fragments (1st and 2nd of I562E and D614R) were cloned using paired primers *BbCRPA*-F/*Bb* (*I562E*)-first-R (I562E-1st), *Bb* (*I562E*)-second-F/*BbCRPAN*-R (I562E-2nd), *BbCRPA*-F/*Bb* (*D614R*)-first-R (D614R-1st), *Bb* (*D614R*)-second-F/*BbCRPAN*-R (D614R-2nd) *via* PCR (PrimeSTAR MAX Premix). The full-length fragments (1st + 2nd) of I562E and D614R were integrated by overlap extension PCR. For BbCrpa N/C-terminus deletion and C-terminus site-directed mutagenesis, the target fragments were cloned with primer pairs *Bb* (Δ*N*)-F/*BbCRPAN-R* (ΔB^{N}), *BbCRPA*-F/*Bb* (Δ*C*)-R (ΔB^{C}), *BbCRPA*-F/*Bb* (Δ*C1325-1359*)-R ($\Delta B^{C1325\text{-}1359}$), *BbCRPA*-F/*Bb* (Δ*C1326-1359*)-R ($\Delta B^{C1326\text{-}1359}$), *BbCRPA*-F/*Bb* (*1325*)-R (Y1325A), *BbCRPA*-F/*Bb* (*1325-1341*)-R (Y1325A-Y1341A), *BbCRPA*-F/*Bb* (*1325-1350*)-R (Y1325A-Y1350A), *BbCRPA*-F/*Bb* (*1341-1350*)-R (Y1341A-Y1350A), *BbCRPA*-F/*Bb* (*1325-1341-1350*)-R (Y1325A-Y1341A-Y1350A). All the PCR products were digested with *Not*I and *Bam*HI and then inserted into the modified PUC-T vector, making it sandwiched by *B. bassiana gpdB*^{1153} promoter and *A. nidulans trpC* terminator, respectively. Then, all vectors were digested with *Xba*I and *Spe*I, and then inserted into pK2-*Sur*. The resulting vectors were transformed into *A. tumefaciens* AGL-1 and subsequently used to transform Δ*BbCRPA*.

For the N/C-terminal tail exchange between BbCrpa and Drs2p, BbCrpa full length sequence (BFL), BbCrpa N-terminus (B^{N}), transmembrane domains (B^{TMD}), C-terminus (B^{C}) were cloned using paired primers *BbCRPAN*-F/*BbCRPAN*-R, *BbCRPA*-F/*BbN*-R, *BbTMD*-F/*BbTMD*-R, *BbC*-F/*BbCRPA*-R, respectively. Drs2p full

length sequence (DFL), Drs2p N-terminus (D^{N}), transmembrane domains (D^{TMD}), C-terminus (D^{C}) were cloned from *Saccharomyces cerevisiae* cDNA using paired primers *DRS2*-F/*DRS2*-R, *DRS2*-F/*DRS2N*-R, *DRS2TMD*-F/*DRS2TMD*-R, *DRS2C*-F/*DRS2*-R, respectively. Overlap extension PCR was performed for the assemblage of different fragments (B^{N}-D^{TMD}-D^{C}, D^{N}-D^{TMD}-B^{C}, B^{N}-D^{TMD}-B^{C}). All the PCR products were digested by *Not*I-*Bam*HI or *Not*I, and then inserted into modified pUC-T vector, making it sandwiched with *B. bassiana gpdB*^{1153} promoter, and *A. nidulans trpC* terminator, respectively. All the integrate expression elements were cloned with primers *P2*-F/*T2*-R and the products were digested with *Spe*I and inserted into pK2-*Sur.* The resulting vectors were used for Δ*BbCRPA* transformation.

Construction of eGFP/mRFP fusion proteins

For N-terminal tagging with eGFP, the coding sequence of BbCrpa was cloned from *B. bassiana* cDNA using primer pair *BbCRPAN*-F/*BbCRPAN*-R and digested with *Not*I and *Bam*HI, and then inserted into the modified PUC-T vector to form PUC-*BbCRPA*. The coding sequence of enhanced green fluorescent protein (eGFP) was amplified from plasmid eGFP-C1 (6084-1, Clontech) using primers *eGFPN*-F/*eGFPN*-R. The resultant fragment was treated with *Not*I, and then cloned into the accomplished vector PUC-*BbCRPA* to generate PUC-*eGFP*::*BbCRPA*, in which the expression of *eGFP*::*BbCRPA* is driven by *B. bassiana gpdB*^{1153} promoter and stopped by *A. nidulans trpC* terminator. Treated the vector with *Xba*I and *Spe*I, and the resultant fragement was inserted into pK2-*Sur* and pK2-*Bar*, respectively. The resulting vectors were transformed into Δ*BbCRPA* and wild-type *B. bassiana*, respectively. For

664 N-terminal tagging with mRFP (monomeric red fluorescent protein), the coding
665 sequences of mRFP was cloned from plasmid p1793 (Pantazopoulou and Peñalva,
666 2009) with primer pair *mRFP*N-F/*mRFP*N-R and *BbCRPA* was cloned using *B.*
667 *bassiana* cDNA as template with primer pair *BbCRPA* (*mF*)-F/*BbCRPAN*-R. The PCR
668 products were fused by overlap extension PCR to link *mFRP* and *BbCRPA* together.
669 The fusing fragement was digested with *Not*I and *Bam*HI, and then inserted into the
670 modified PUC-T to form PUC-*mRFP*::*BbCRPA*, the expression of which is driven by
671 *B. bassiana gpdB*^{1153} promoter and sotpped by *A. nidulans trpC* terminator. Then, the
672 vector was digested with *Xba*I and *Spe*I, and inserted into pK2-*Sur.* The resulting
673 vector was used for the transformation of Δ*BbCRPA*.

674 For labeling late Golgi, *gpdA*^{mini}::*mRFP*::*PH*^{OSBP} was amplified from plasmid
675 p1793 using primers *mPH*-F and *mPH*-R. The product was digested with *Xba*I, and
676 then inserted into pK2-*Sur.* The resulting vector was transformed into the wild-type
677 and *eGFP::BbCRPA* strains, respectively.

678 For labeling EE (early endosome) and LE (late endosome), *B. bassiana* endogenous
679 small GTPases BbRab5 and BbRab7 were cloned using the primer pairs
680 *BbRab5*-F/*BbRab5*-R and *BbRab7*-F/*BbRab7*-R, respectively. The coding sequence of
681 mRFP was amplified from plasmid p1793 using primers *mRFPN*-F/*mRFPN*-R. The
682 fragment of mRFP was fused with BbRab5/BbRab7 by overlap extension PCR. The
683 resulting fusion sequences were cloned into modified PUC-T vector to form
684 PUC-*mRFP*::*BbRab5* and PUC-*mRFP*::*BbRab7*, respectively. PUC-*mRFP*::*BbRab5*
685 was digested with *Xba*I and *Spe*I, and then inserted into pK2-*Sur.* The fragment of

686 *gpdB*^{1153}::*mRFP*::*BbRab7*::*trpC* was cloned from PUC-*mRFP*::*BbRab7* using primers
687 *P1*-F/*T1*-R. The resulting PCR product was digested with *Xba*I, and then inserted into
688 pK2-*Sur.* All the resulting vectors were transformed into *eGFP*::*BbCRPA* strain and
689 wild-type *B. bassiana*.

690 For Drs2p localization observation, the coding sequences of eGFP and Drs2p were
691 amplified from plasmid eGFP-C1 and *Saccharomyces cerevisiae* cDNA using primer
692 pairs *eGFPN*-F/*eGFP* (*NF*)-R and *DRS2* (Fu)-F/*DRS2*-R, respectively. eGFP and
693 Drs2p were fused by overlap extension PCR. The resulting product, *eGFP*::*DRS2*,
694 was digested with *Not*I, and then inserted into the modified PUC-T. The fragment of
695 *gpdB*^{1153}::*eGFP*::*DRS2*::*trpC* was cloned from PUC-*eGFP*::*DRS2* using primers
696 *P2*-F/*T2*-R. The resulting product was digested with *Spe*I, and then inserted into
697 pK2-*Sur.* The resulting vector was transformed into Δ*BbCRPA*.

698 For BbCrpa full length N-terminus ($B^{N1\text{-}268}$) tagging with mRFP, the coding
699 sequences of $B^{N1\text{-}268}$ and mRFP were generated by PCR with primer pairs
700 *BbCRPA*N-F/*N268*-R, *mRFP*-F/*mRFP*-R, respectively. The products were fused by
701 overlap extension PCR. The fusion sequence was then digested with *Not*I and *Bam*HI,
702 and inserted into the modified PUC-T to form PUC-$B^{N1\text{-}268}$::mRFP between *B.*
703 *bassiana gpdB*^{1153} promoter and *A. nidulans trpC* terminator. For tagging B^{N0},
704 $B^{N258\text{-}268}$, $B^{N258\text{-}268\ (K264A)}$, and $B^{N259\text{-}268}$ with mRFP, the coding sequences of them
705 were cloned by PCR with primer pairs *mRFP*N-F/*mRFP*-R, *N258-268*-F/*mRFP*-R,
706 *N258-268* (*K-A*)-F/*mRFP*-R, *N259-268*-F/*mRFP*-R using plasmid
707 PUC-$B^{N1\text{-}268}$::mRFP as template. All the PCR products were digested with *Not*I and

*Bam*HI, and then inserted into the modified PUC-T. These modified PUC-T vectors were digested with *Xba*I and *Spe*I, and then inserted into pK2-*Sur*. Finally, the resulting vectors were transformed into eGFP::BbCrpa strain.

Ectopic expression of *BbCRPA* in *V. dahliae*

For *V. dahliae* transformation, BbCrpa coding sequence was cloned with primer pair *BbCRPA*N-F/*BbCRPA*N-R and digested with *Not*I and *Bam*HI. The resultant fragment was inserted into the modified PUC-T vector. Then, the vector was digested with *Xba*I and *Spe*I. The resulting fragement was inserted into pK2-*Hyg*, a vector with hygromycin B (10687010, Thermo Scientific)-resistance-encoding gene as a selection marker. The resulting vector was transformed into *A. tumefaciens* AGL-1 and subsequently used to transform the wild-type *V. dahliae* as described previously (Zhou et al., 2013).

Ectopic expression of *BbCRPA* in Arabidopsis and cotton

For Arabidopsis and cotton transformation, BbCrpa coding sequence was cloned by PCR with primer pair *pBbCRPA*-F/*pBbCRPA*-R. The product was digested with *Bam*HI/*Spe*I, and inserted into modified pCAMBIA2300 (VT1383, YouBio) (PLGN) between cauliflower mosaic virus *35S* promoter and *A. tumefaciens Nos* terminator. The resulting vector was transformed into *A. tumefaciens* GV3101 and LBA4404 for Arabidopsis (Col-0) and cotton transformation, respectively.

Phenotypic assays

Fungi were grown on CZP (agar) (*B. bassiana*) or CZA (*B. bassiana*) or PDA (*V.*

dahliae) supplemented with CsA or FK506 typically by inoculation of 3 μl of conidial suspensions (1×10^7 conidia/ml in 0.05% tween-80) onto the center of agar plates. Plates were incubated at 26 ºC for about 10-14 days. For growth inhibition rates assays of different strains, the data were shown as [colony diameter CZP/CZA supplemented with CsA/FK506]/[colony diameter CZP/CZA].

Gene expression analysis

For *BbCRPA* expression analysis, 1 μg total RNA was reverse-transcribed using PrimeScript RT reagent Kit (RR047A, TaKaRa). Quantitative RT-PCR (qRT-PCR) was performed using a CFX96 Real-Time System (Bio-Rad). PCR reactions were performed in 96-well plates as follows: 10 μl iQSYBR Green Supermix (1708882, Bio-Rad), 500 nM forward and reverse primers, and 1 μl 1:7 diluted cDNA template. All experiments were performed thrice. *γ-actin* (for *B. bassiana*), *AtActin*2 (for Arabidopsis) and *GhHis*3 (for cotton) were used as the internal reference. The regular PCR cycling conditions were as follows: 3 min at 95 ºC, followed by 40 cycles of 10 s at 95 ºC, 30 s at 56 ºC and 30 s at 72 ºC. In order to verify the specificity of the primers, a melt curve analysis was performed for quality assurance. Relative expression of the target gene was normalized to the quantity of the reference gene (normalized fold expression) and processed in CFX Manager 3.1 software (BioRad). Primers used for qRT-PCR analysis are given in Supplemental Information Table supplement 1.

Fluorescence labeling of CsA, FK506, and CIA

CsA and FK506 were labeled with 5-Carboxyfluorescein (5-FAM, HY-66022, MCE). Cinnamyl acetate (CIA, 166170, Sigma-Aldrich) was labeled with fluorescein isothiocyanate (FITC, HY-66019, MCE). The labeled molecules were produced by Fanbo Biochemicals Co. Ltd.. (Haidian HighTech Business Park, Beijing, China).

Sample preparation for imaging

All experiments for imaging of *B. bassiana* were performed in CZB medium, with external supplements added as needed. All the fluorescent strains were precultured in CZB (200 rpm, 26 °C), 48-72 h aged hyphae were harvested from CZB medium (10, 000 rpm, 5 min, 4 °C) and resuspended in PBS (NaCl 8 g/l, KCl 0.2 g/l, $Na_2HPO_4 \cdot 12 H_2O$ 3.63 g/l, KH_2PO_4 0.24 g/l, pH 7.4, typically 0.1 ml). For video acquisition, 48-72 h aged hyphae were harvested and observed second by second. FM4-64 (F34653, Thermo Scientific) was used to stain the membrane of vacuole, prevacuolar (PVC)/multivesicular body (MVB) and vesicle, and the protocol was as described previously (Lewis et al., 2009) with slight modification. Briefly, samples were resuspended into HBSS (Hank's balanced salt solution, NaCl 8 g/l, KCl 0.4 g/l, KH_2PO_4 0.06 g/l, $Na_2HPO_4 \cdot 12H_2O$ 0.121 g/l, Glucose 1 g/l, pH 7.2) containing a final concentration of 8 μM FM4-64 and then incubated at 4 °C for 40-60 min. For FM1-43 (T35356, Thermo Scientific) staining, samples were resuspended into HBSS containing a final concentration of 20 μM and then incubated at 4 °C for 60 min. For the observation of 5-FAM labeled CsA and FK506 in the fungus, the labeled molecules were added to the CZB medium to a final concentration of 7.5 μg /ml (CsA) and 6 μg/ml (FK506), respectively, and incubated with fungal cells for 48-72 hours.

Finally, the samples were washed with PBS twice for imaging. For the observation of FITC labeled CIA in the plant, Arabidopsis seedlings were incubated in liquid Murashige and Skoog medium (MS, M519, Phytotech) (1.5% [w/v] Sucrose, pH 5.8) containing FITC-CIA (5 μg/ml) and FM4-64 (4 μM) at 22 ^{o}C for 8 hours and the samples were washed with ddH_2O 3-4 times for imaging.

Image acquisition

For confocal microscopy, an inverted confocal laser scanning microscope (FV1000, Olympus) was used. For the observation of fluorescent signals of eGFP, 5-FAM, and FITC, an argon ion laser (Ex = 488 nm, Em = 515-530 nm) was used. For the observation of mRFP and FM4-64, fluorescent signals were acquired using a He-Ne laser (Ex = 559 nm, Em = 570-670 nm). Finally, all the confocal images were captured with FV10-ASW 3.0 Viewer software (Olympus).

Insect bioassays

Fourth-instar larvae of *Galleria mellonella* were used as target insects for bioassays. Larvae were immersed into suspensions (2×10^7 conidia/ml in 0.05% tween-80) derived from Δ*BbCRPA* and the wild-type for 15 s. Excess solution was removed by treating with paper towel. All treated larvae were transferred into growth chamber at 26 °C for 15 h:9 h (light:dark cycle) with 70% relative humidity. The mortality was recorded every 12 h. Each treatment was performed in triplicate with 30-40 insects with at least two independent batches on conidia. Kaplan-Meyer curves were used for analyzing the survival data and a log rank test was used to analyze the difference

between Δ*BbCRPA* and the wild-type.

Western blot and immunoprecipitation

For the immunoprecipitation (IP) and immunoblot assays, the total protein was extracted according to the extraction kit (BB-3136, BestBio). IP was performed according to the manufacturer's protocol (SA079001, Smart-lifesciences) with silght modification. Briefly, the protein complexes were isolated by binding to the anti-RFP affinity beads 4FF, followed by two washes with balanced solution (50 mM Tris, 0.15 M NaCl, pH 7.4). Finally, 200 μl PBS with 5 × SDS-PAGE loading buffer was added to the complexes and incubated at 95 ℃ for 10 minutes and the affinity beads were collected by centrifugation (5, 000 g , 1 min). The supernatants that contain the eluted targets were analyzed by immunoblotting with anti-Ub (ubiquitin, PTM-1107, PTM-BIO) and anti-RFP antibodies (MA5-15257, Thermo Scientific).

Southern blot

Southern blot was performed according to DIG High Prime DNA Labelling and Detection Starter Kit II (11585614910, Roche). Briefly, 30 μg DNA from the leaves of wild-type and transgenic plants were digested with *Hin*dIII and subjected to DNA electrophoresis with 0.8% agarose gel. Probe was prepared from the purified PCR product of the *BbCRPA* gene. The labelling of probe, hybridization and detection were performed according to the manufacturer's instructions. The primer pair used for southern blot is given in Supplementary file 4.

Plant transformation and resistance assays for disease or CIA

Genetic transformation of Arabidopsis and identification of the transformants were performed as described previously (Clough and Bent, 2010; Harrison et al., 2006). The transformation of cotton (*cv.* Jimian 14) was performed according to the method as described previously (Luo et al., 2007). For disease resistance assays of Arabidopsis, each Arabidopsis plant (4-5 leaves) was inoculated with 3 ml *V. dahliae* spore suspension (2×10^8 spores/ml, V991 strain) and then all Arabidopsis plants were transferred into growth chamber at 22 °C for 16 h:8 h (light:dark cycle) with 70% relative humidity. The resistance of the plants to *V. dahliae* was evaluated 21 days later after inoculation. For disease resistance assays of cotton, 10-day-old cotton seedlings were treated with *V. dahliae* (10^7 spores/ml, V991 strain) according to the method as described previously (Fradin et al., 2009) and then the cotton plants were transferred into growth chamber at 26 °C for 16 h:8 h (light:dark cycle) with 70% relative humidity. The disease index of the plants to *V. dahliae* was evaluated 14 days after inoculation. The symptom of infected plants was evaluated by different grades of disease: 0, health plant; 1, 0-25% chlorotic or necrotic leaves; 2, 25-50% chlorotic or necrotic leaves; 3, 50-75% chlorotic or necrotic leaves; 4, 75-100% chlorotic or necrotic leaves or no leaf left or dead plant. The disease index (DI) was calculated according to the following formula: DI = [∑(disease grades × number of infected plants)/(total checked plants × 4)] × 100 (Zhang et al., 2012). The disease resistance experiments were performed three times with more than 15 plants for Arabidopsis and 30 plants for cotton each time. For CIA resistance assays of Arabidopsis, Arabidopsis seeds were incubated on MS plates supplemented with either 0.5% DMSO (control)

836 or CIA (50 μg/ml) for 14 days.

837 **Statistical analyses**

838 Statistical analyses were performed with a Student's *t* test or a log rank test.
839 Significance was defined as **p < 0.01; ***p < 0.001; ****p < 0.0001. Differences with
840 a *P* value of 0.05 or less were considered significant. For insect survival study,
841 Kaplan-Meier survival curve was generated and analyzed for statistical significance
842 with GraphPad 5.0. Statistical details for each experiment can be found in the Figure
843 Legends.

844 ## Acknowledgments

845 This work was supported by the Chinese Ministry of Science and Technology of
846 China (Grant 2016YFD0100505), National Transgenic New Species Breeding Major
847 Project of China (2016ZX08005-003-004 to Y.P), and National Major Project of
848 Breeding of China (2018YFD0100403 to X.L). We thank Prof. Qixiang Guo (School
849 of Chemistry and Chemical Engineering, Southwest University, Chongqing, China)
850 for his help in CsA/FK506 labeling, and Dr. Zhibing Luo (Biotechnology Research
851 Center, Southwest University, Chongqing, China) for his assistance in the
852 construction of T-DNA insertion mutant pool in *B. bassiana*. We are grateful to Dr.
853 Miguel A. Peñalva (Department of Physical and Chemical Biology, Centro de
854 Investigaciones Biológicas, Consejo Superior de Investigaciones Científicas, Ramiro
855 de Maeztu 9, 28040 Madrid, Spain) for providing plasmid p1793, Prof. Weiguo Fang
856 (Institute of Microbiology, Zhejiang University, Hangzhou, China) for the gift of *M.*
857 *anisopliae* strain, Guiliang Jian (Institute of Plant Protection, Chinese Academy of

Agricultural Sciences, Beijing, China) for the gift of *V. dahliae* strain V991, and Prof. Zhiying Ma (State Key Laboratory of North China Crop Improvement and Regulation, North China Key Laboratory for Crop Germplasm Resources of Education Ministry, Hebei Agricultural University, Hebei, China) for the gift of *Gossypium hirsutum*, *cv.* Jimian 14.

Additional information

Funding

Funder	Grant reference number	Author
Chinese Ministry of Science and Technology of China	2016YFD0100505	Yan Pei
National Transgenic New Species Breeding Major Project of China	2016ZX08005-003-004	Yan Pei
National Major Project of Breeding of China	2018YFD0100403	Xianbi Li

The funders had no role in study design, data collection and interpretation, or the decision to submit the work for publication.

Author contributions

Yujie Li, Hui Ren, Conceptualization, Data curation, Software, Formal analysis, Validation, Investigation, Visualization, Writing-original draft, Writing-review and editing; Fanlong Wang, Resources, Data curation, Software, Formal analysis,

Investigation, Visualization, Methodology; Jianjun Chen, Lian Ma, Yang Chen, Data curation, Software, Formal analysis, Validation, Methodology; Xianbi Li, Data curation, Software, Validation, Investigation, Funding acquisition; Yanhua Fan, Dan Jin, Data curation, Software, Validation, Investigation, Methodology; Lei Hou, Yonghong Zhou, Software, Validation, Investigation, Methodology; Nemat O. Keyhani, Conceptualization, Resources, Validation, Writing-review and editing; Yan Pei, Conceptualization, Resources, Formal analysis, Supervision, Funding acquisition, Investigation, Project administration, Writing-review and editing

Additional files

Supplementary files

- Supplementary file 1. Time-lapse imaging of the trajectory of eGFP::BbCrpa (green) and vesicle (red) labeled by FM4-64. Time to acquire one image pair was 1 s. Scale bar, 5 μm.
- Supplementary file 2. Time-lapse imaging of the trajectory of eGFP::BbCrpa (green) and vesicle (red) derived from TGN which was labeled by mRFP::PH^{OSBP} (red). Time to acquire one image pair was 1 s. Scale bar, 5 μm.
- Supplementary file 3. Loss of autophagy-related protein BbAtg1, adaptor protein BbAP-1, or coat protein clathrin does not affect CsA resistance.
- Supplementary file 4. Primers used in this study.
- Supplementary file 5. Key resources table.

Competing interests

The authors declare that no competing interests exist.

References

Barreiro C, Prieto C, Sola-Landa A, Solera E, Martinez-Castro M, Perez-Redondo R, Garcia-Estrada C, Aparicio JF, Fernandez-Martinez LT, Santos-Aberturas J, Salehi-Najafabadi Z, Rodriguez-Garcia A, Tauch A, Martin JF. 2012. Draft genome of Streptomyces tsukubaensis NRRL 18488, the producer of the clinically important immunosuppressant tacrolimus (FK506). *Journal of Bacteriology* **194:**3756-3757. DOI: https://doi.org/10.1128/JB.00692-12, PMID: 22740677

Barz S, Kriegenburg F, Henning A, Bhattacharya A, Mancilla H, Sanchez-Martin P, Kraft C. 2020. Atg1 kinase regulates autophagosome-vacuole fusion by controlling SNARE bundling. *EMBO Reports*. **21:**e51869. DOI: https://doi.org/10.15252/embr.202051869, PMID: 33274589

Bauer K, Kretzschmar AK, Cvijic H, Blumert C, Loffler D, Brocke-Heidrich K, Schiene-Fischer C, Fischer G, Sinz A, Clevenger CV, and Horn F. 2009. Cyclophilins contribute to Stat3 signaling and survival of multiple myeloma cells. *Oncogene*. **28:**2784-2795. DOI: https://doi.org/10.1038/onc.2009.142, PMID: 19503092

Baxter BK, Abeliovich H, Zhang X, Stirling AG, Burlingame AL and Goldfarb DS. 2005. Atg19p ubiquitination and the cytoplasm to vacuole trafficking pathway in yeast. *Journal of Biological Chemistry* **280:**39067-39076. DOI: https://doi.org/ 10.1074/jbc.M508064200, PMID: 16186126

Beauchesne PR, Chung NS, Wasan KM. 2007. Cyclosporine A: a review of current

oral and intravenous delivery systems. *Drug Development and Industrial Pharmacy* **33:**211-220. DOI: https://doi.org/10.1080/03639040601155665, PMID: 17454054

Berthiller F, Crews C, Dall'Asta C, Saeger SD, Haesaert G, Karlovsky P, Oswald IP, Seefelder W, Speijers G, Stroka J. 2013. Masked mycotoxins: a review. *Molecular Nutrition & Food Research* **57:**165-186. DOI: https://doi.org/10.1002/mnfr.201100764, PMID: 23047235

Borel JF, Feurer C, Gubler HU, and Stähelin H. 1976. Biological effects of cyclosporin A: a new antilymphocytic agent. *Agents and Actions* **6:**468-475. DOI: https://doi.org/10.1007/bf01973261, PMID: 8969

Borel JF, Gunn HC. 1986. Cyclosporine as a New Approach to Therapy of Autoimmune Diseases. *Annals of the New York Academy of Sciences* **475:**307-319. DOI: https://doi.org/ 10.1111/j.1749-6632.1986.tb20879.x, PMID: 3538973

Brakhage, AA. 2013. Regulation of fungal secondary metabolism. *Nature Reviews Microbiology* **11:**21-32. DOI: https://doi.org/10.1038/nrmicro2916, PMID: **23178386**

Brazin KN, Mallis RJ, Fulton DB, Andreotti AH. 2002. Regulation of the *tyrosine kinase Itk by the peptidyl-prolyl isomerase cyclophilin A. PNAS* **99:**1899-1904. DOI: https://doi.org/10.1073/pnas.042529199, PMID: 11830645

Carrera A, Moos J, Ning XP, Gerton GL, Tesarik J, Kopf GS, Moss SB. 1996. Regulation of protein tyrosine phosphorylation in human sperm by a calcium/calmodulin-dependent mechanism: identification of A kinase anchor proteins as major substrates for tyrosine phosphorylation. *Developmental*

Biology **180:**284-296. DOI: https://doi.org/10.1006/dbio.1996.0301, PMID: 8948591

Chan CP, Gallis B, Blumenthal DK, Pallen CJ, Wang JH, Krebs EG. 1986. Characterization of the phosphotyrosyl protein phosphatase activity of calmodulin-dependent protein phosphatase. *Journal of Biological Chemistry* **261:**9890-9895. DOI: https://doi.org/10.1007/BF00004214, PMID: 2426255

Chanda A, Roze LV, Kang S, Artymovich KA, Hicks GR, Raikhel NV, Calvo AM, Linz JE. 2009. A key role for vesicles in fungal secondary metabolism. *PNAS* **106:**19533-19538. DOI: https://doi.org/ 10.1073/pnas.0907416106, PMID: 19889978

Ciechanover A. 1998. The ubiquitin-proteasome pathway: on protein death and cell life. *EMBO Journal* **17:**7151-7160. DOI: https://doi.org/10.1093/emboj/17.24.7151, PMID: 9857172

Clough SJ, Bent AF. Bent. 2010. Floral dip: a simplified method for *Agrobacterium*-mediumted transformation of *Arabidopsis thaliana*. *The Plant. Journal*. **16:**735-743. DOI: https://doi.org/10.1046/j.1365-313x.1998.00343.x, PMID: 10069079

Coleman J, Blake-Kalff M, Davies E. 1997. Detoxification of xenobiotics by plants: chemical modification and vacuolar compartmentation. *Trends in Plant Science* **2:**144-151. DOI: https://doi.org/10.1016/S1360-1385(97)01019-4

Coleman JA, Quazi F, Molday RS. 2013. Mammalian P4-ATPases and ABC transporters and their role in phospholipid transport. *Biochimica et Biophysica Acta* **1831:**555-574. DOI: https://doi.org/10.1016/j.bbalip.2012.10.006, PMID:

23103747

De Matteis MA, Vicinanza M, Venditti R, Wilson C. 2013. Cellular assays for drug discovery in genetic disorders of intracellular trafficking. *Annual Review of Genomics and Human Genetics* **14:**159-190. DOI: https://doi.org/10.1146/annurev-genom-091212-153415, PMID: 23662666

D'Mello JPF, Placinta CM, Macdonald AMC. 1999. *Fusarium* mycotoxins: a review of global implications for animal health, welfare and productivity. *Animal Feed Science and Technology* **80:**183-205. DOI: https://doi.org/10.1016/s0377-8401(99)00059-0

Dimartini A, Trzepacz PT, Daviss SR. 1996. Prospective study of FK506 side effects: Anxiety or akathisia? *Biological Psychiatry* **40:**407-411. DOI: https://doi.org/10.1016/0006-3223(95)00395-9, PMID: 8874843

Dreyfuss M, Härri E, Hofmann H, Kobel H, Pache W, Tscherter H. 1976. Cyclosporin A and C. *European Journal of Applied Microbiology* **3:**125-133. DOI: https://doi.org/10.1007/BF00928431

Fang WG, Leng B, Xiao YH, Jin K, Ma JC, Fan YH, Feng J, Yang XY, Zhang YJ, Pei Y. 2005. Cloning of *Beauveria bassiana* chitinase gene Bbchit1 and its application to improve fungal strain virulence. *Applied and Environmental Microbiology* **71:**363-370. DOI: https://doi.org/10.1128/AEM.71.1.363-370.2005, PMID: 15640210

Fang WG, Zhang YJ, Yang XY, Zheng XL, Duan H, Li Y, Pei Y. 2004. *Agrobacterium tumefaciens*-mediated transformation of *Beauveria bassiana* using an herbicide resistance gene as a selection marker. *Journal of*

Invertebrate Pathology **85:**18-24. DOI: https://doi.org/10.1016/j.jip.2003.12.003, PMID: 14992856

Faure C, Corvol JC, Toutant M, Valjent E, Hvalby O, Jensen V, El Messari S, Corsi JM, Kadare G, Girault JA. 2007. Calcineurin is essential for depolarization-induced nuclear translocation and tyrosine phosphorylation of PYK2 in neurons. *Journal of Cell Science* **120:**3034-3044. DOI: https://doi.org/ 10.1242/jcs.009613, PMID: 17684059

Fleming, A. 1944. The discovery of penicillin. *British Medical Journal*. **2:**792-792. DOI: https://doi.org/10.1093/oxfordjournals.bmb.a071032

Fradin EF, Thomma BP. 2006. Physiology and molecular aspects of Verticillium wilt diseases caused by *V. dahliae* and *V. albo-atrum*. *Molecular Plant Pathology* **7:**71-86. DOI: https://doi.org/10.1111/j.1364-3703.2006.00323.x, PMID: 20507429

Fradin EF, Zhang Z, Juarez Ayala JC, Castroverde CD, Nazar RN, Robb J, Liu CM, Thomma BP. 2009. Genetic dissection of Verticillium wilt resistance mediated by tomato Ve1. *Plant Physiology* **150:**320-332. DOI: https://doi.org/10.1104/pp.109.136762, PMID: 19321708

Ghelis, T. 2011. Signal processing by protein tyrosine phosphorylation in plants. *Plant Signaling & Behavior* **6:**942-951. DOI: https://doi.org/10.4161/psb.6.7.15261, PMID: 21628997

Guada M, Beloqui A, Kumar MN, Preat V, Dios-Vieitez Mdel C, Blanco-Prieto MJ. 2016. Reformulating cyclosporine A (CsA): More than just a life cycle management strategy. *Journal of Controlled Release* **225:**269-282. DOI: https://doi.org/10.1016/j.jconrel.2016.01.056, PMID: 26829101

Gupta AK, Ellis CN, Goldfarb MT, Cooper KD, Rocher L, Brown MD, Baadsgaard O, Voorhees JJ. 1989. Cyclosporine A. *Clinics in Dermatology* **7:**98-110. DOI: https://doi.org/10.1016/0738-081x(89)90011-4, PMID: 2680025

Hankins HM, Baldridge RD, Xu P, Graham TR. 2015. Role of flippases, scramblases and transfer proteins in phosphatidylserine subcellular distribution. *Traffic*. **16:**35-47. DOI: https://doi.org/10.1111/tra.12233, PMID: 25284293

Hansen GH, Rasmussen K, Niels-Christiansen LL, Danielsen EM. 2009. Endocytic trafficking from the small intestinal brush border probed with FM dye. *American Journal of Physiology-Gastrointestinal and Liver Physiology* **297:**G708-715. DOI: https://doi.org/10.1152/ajpgi.00192.2009, PMID: 19679822

Haranishimura I, Shimada T, Hatano K, Takeuchi Y, Nishimura M. 1998. Transport of storage proteins to protein storage vacuoles is mediated by large precursor-accumulating vesicles. *Plant Cell*. **10:**825-836. DOI: https://doi.org/10.1105/tpc.10.5.825, PMID: 9596640

Harrison SJ, Mott EK, Parsley K, Aspinall S, Gray JC, Cottage A. 2006. A rapid and robust method of identifying transformed *Arabidopsis thaliana* seedlings following floral dip transformation. *Plant Methods* **2:**19. DOI: https://doi.org/10.1186/1746-4811-2-19, PMID: 17087829

Howard JP, Hutton JL, Olson JM, Payne GS. 2002. Sla1p serves as the targeting signal recognition factor for NPFX(1,2)D-mediated endocytosis. *Journal of Cell Biology* **157:**315-326. DOI: https://doi.org/10.1083/jcb.200110027, PMID: 11940605

Hua Z, Fatheddin P, Graham TR. 2002. An essential subfamily of Drs2p-related

P-type ATPases is required for protein trafficking between Golgi complex and endosomal/vacuolar system. *Molecular Biology of the Cell* **13:**3162-3177. DOI: https://doi.org/10.1091/mbc.e02-03-0172, PMID: 12221123

Hunt J, Morshead CM. 2010. Cyclosporin A Enhances Cell Survival in Neural Precursor Populations in the Adult Central Nervous System. *Molecular and Cellular Pharmacology* **2:**81-88. DOI: https://doi.org/10.4255/mcpharmacol.10.11

Kaeberlein M. 2013. mTOR Inhibition: From Aging to Autism and Beyond. *Scientifica (Cairo)*. **2013:**849186. DOI: https://doi.org/10.1155/2013/849186, PMID: 24379984

Kang CB, Hong Y, Dhe-Paganon S, Yoon HS. 2008. FKBP family proteins: immunophilins with versatile biological functions. *Neurosignals*. **16:**318-325. DOI: https://doi.org/10.1159/000123041, PMID: 18635947

Kaufmann A, Beier V, Franquelim HG, Wollert T. 2014. Molecular mechanism of autophagic membrane-scaffold assembly and disassembly. *Cell*. **156:**469-481. DOI: https://doi.org/10.1016/j.cell.2013.12.022, PMID: 24485455

Keen NT, Long M, Erwin DC. 1972. Possible involvement of a pathogen-produced protein-lipopolysaccharide complex in Verticillium wilt of cotton. *Physiological Plant Pathology* **2:**317-333. DOI: https://doi.org/10.1016/S0048-4059(72)80006-7

Keller NP. 2015. Translating biosynthetic gene clusters into fungal armor and weaponry. *Nature Chemical Biology* **11:**671-677. DOI: https://doi.org/10.1038/nchembio.1897, PMID: 26284674

Keller NP, Turner G, Bennett JW. 2005. Fungal secondary metabolism-from biochemistry to genomics. *Nature Reviews Microbiology* **3:**937-947. DOI: https://doi.org/10.1038/nrmicro1286, PMID: 16322742

Laouane H, Lazrek HB, Sedra MH. 2011. Synthesis and toxicity evaluation of cinnamyl acetate: a new phytotoxin produced by a strain of *Verticillium dahliae* pathogenic on olive tree. *International Journal of Agriculture and Biology* **13:**444-446. DOI: https://doi.org/10.1111/j.1744-7348.2010.00451.x

Lewis MW, Robalino IV, Keyhani NO. 2009. Uptake of the fluorescent probe FM4-64 by hyphae and haemolymph-derived in vivo hyphal bodies of the entomopathogenic fungus *Beauveria bassiana*. *Microbiology*. **155:**3110-3120. DOI: https://doi.org/10.1099/mic.0.029165-0, PMID: 19542008

Liu JS, Farmer JD, Lane WS, Friedman JS, Weissman IL, Schreiber SL. 1991. Calcineurin is a common target of cyclophilin-cyclosporin A and FKBP-FK506 complexes. *Cell*. **66:**807-815. DOI: https://doi.org/10.1016/0092-8674(91)90124-h, PMID: 1715244

Liu K, Hua Z, Nepute JA, Graham TR. 2007. Yeast P4-ATPases Drs2p and Dnf1p are essential cargos of the NPFXD/Sla1p endocytic pathway. *Molecular Biology of the Cell*. **18:**487-500. DOI: https://doi.org/10.1091/mbc.e06-07-0592, PMID: 17122361

Liu K, Surendhran K, Nothwehr SF, Graham TR. 2008. P4-ATPase requirement for AP-1/clathrin function in protein transport from the trans-Golgi network and early endosomes. *Molecular Biology of the Cell* **19:**3526-3535. DOI: https://doi.org/10.1091/mbc.e08-01-0025, PMID: 18508916

Lopez-Ilasaca M, Schiene C, Kullertz G, Tradler T, Fischer G, Wetzker R. 1998. Effects of FK506-binding protein 12 and FK506 on autophosphorylation of epidermal growth factor receptor. *Journal of Biological Chemistry*. **273:**9430-9434. DOI: https://doi.org/10.1074/jbc.273.16.9430, PMID: 9545268

Lopez-Marques RL, Theorin L, Palmgren MG, Pomorski TG. 2014. P4-ATPases: lipid flippases in cell membranes. *Pflugers Archiv-european Journal of Physiology* **466:**1227-1240. DOI: https://doi.org/10.1007/s00424-013-1363-4, PMID: 24077738

Luo M, Xiao YH, Li XB, Lu XF, Deng W, Li DM, Hou L, Hu MY, Li Y, Pei Y. 2007. GhDET2, a steroid 5alpha-reductase, plays an important role in cotton fiber cell initiation and elongation. *The Plant Journal* **51:**419-430. DOI: https://doi.org/10.1111/j.1365-313X.2007.03144.x, PMID: 17565582

MacGurn JA, Hsu PC, Emr SD. 2012. Ubiquitin and membrane protein turnover: from cradle to grave. *Annual Review of Biochemistry* **81:**231-259. DOI: https://doi.org/10.1146/annurev-biochem-060210-093619, PMID: 22404628

Margaritis A, Chahal P. 1989. Development of a fructose based medium for biosynthesis of cyclosporin-A by *Beauveria nivea*. *Biotechnology Letters* **11:**765-768. DOI: https://doi.org/10.1007/BF01026093

McMahon HT, Gallop JL. 2005. Membrane curvature and mechanisms of dynamic cell membrane remodelling. *Nature*. **438:**590-596. DOI: https://doi.org/10.1038/nature04396, PMID: 16319878

Meyer R, Slater V, Dubery IA. 1994. A phytotoxic protein-lipopolysaccharide complex produced by *Verticillium dahliae*. *Phytochemistry*. **35:**1449-1453.

DOI: https://doi.org/10.1016/S0031-9422(00)86872-7

Molinari M, Galli C, Norais N, Telford JL, Rappuoli R, Luzio JP, Montecucco C. 1997. Vacuoles induced by Helicobacter pylori toxin contain both late endosomal and lysosomal markers. *Journal of Biological Chemistry* **272:**25339-25344. DOI: https://doi.org/10.1074/jbc.272.40.25339, PMID: 9312153

Odom AR, Muir S, Lim E, Toffaletti DL, Perfect JR, Heitman J. 1997. Calcineurin is required for virulence of *Cryptococcus neoformans*. *EMBO Journal*. **16:**2576-2589. DOI: https://doi.org/10.1093/emboj/16.10.2576, PMID: 9184205

Ownley BH, Griffin MR, Klingeman WE, Gwinn KD, Moulton JK, Pereira RM. 2008. *Beauveria bassiana*: endophytic colonization and plant disease control. *Journal of Invertebrate Pathology* **98:**267-270. DOI: https://doi.org/10.1016/j.jip.2008.01.010, PMID: 18442830

Palmgren MG, Nissen P. 2011. P-type ATPases. *Annual Review of Biophysics* **40:**243-266. DOI: https://doi.org/10.1146/annurev.biophys.093008.131331, PMID: 21351879

Panatala R, Hennrich H, Holthuis JC. 2015. Inner workings and biological impact of phospholipid flippases. *Journal of Cell Science* **128:**2021-2032. DOI: https://doi.org/10.1242/jcs.102715, PMID: 25918123

Pantazopoulou A, Peñalva MA. 2009. Organization and dynamics of the *Aspergillus nidulans* Golgi during apical extension and mitosis. *Molecular Biology of the Cell*. **20:**4335-4347. DOI: https://doi.org/10.1091/mbc.e09-03-0254, PMID: 19692566

Perez C, Gerber S, Boilevin J, Bucher M, Darbre T, Aebi M, Reymond JL, Locher KP. 2015. Structure and mechanism of an active lipid-linked oligosaccharide flippase. *Nature*. **524:**433-438. DOI: https://doi.org/10.1038/nature14953, PMID: 26266984

Pomorski T, Lombardi R, Riezman H, Devaux PF, van Meer G, Holthuis JC. 2003. Drs2p-related P-type ATPases Dnf1p and Dnf2p are required for phospholipid translocation across the yeast plasma membrane and serve a role in endocytosis. *Molecular Biology of the Cell*. **14:**1240-1254. DOI: https://doi.org/10.1091/mbc.e02-08-0501, PMID: 12631737

Poulsen LR, Lopez-Marques RL, McDowell SC, Okkeri J, Licht D, Schulz A, Pomorski T, Harper JF, Palmgren MG. 2008. The Arabidopsis P4-ATPase ALA3 localizes to the golgi and requires a beta-subunit to function in lipid translocation and secretory vesicle formation. *Plant Cell*. **20:**658-676. DOI: https://doi.org/10.1105/tpc.107.054767, PMID: 18344284

Rosenblum K, Schul R, Meiri N, Hadari YR, Zick Y, Dudai Y. 1995. Modulation of protein tyrosine phosphorylation in rat insular cortex after conditioned taste aversion training. *PNAS* **92:**1157-1161. DOI: https://doi.org/10.1073/pnas.92.4.1157, PMID: 7862652

Roth AF, Sullivan DM, Davis NG. 1998. A large PEST-like sequence directs the ubiquitination, endocytosis, and vacuolar degradation of the yeast a-factor receptor. *Journal of Cell Biology* **142:**949-961. DOI: https://doi.org/10.1083/jcb.142.4.949, PMID: 9722608

Rothman JE, Wieland FT. 1996. Protein Sorting by Transport Vesicles. *Science*. **272:**227-234. DOI: https://doi.org/10.1126/science.272.5259.227, PMID:

8602507

Rotin D, Staub O, Haguenauer-Tsapis R. 2000. Ubiquitination and endocytosis of plasma membrane proteins: role of Nedd4/Rsp5p family of ubiquitin-protein ligases. *The Journal of Membrane Biology* **176:**1-17. DOI: https://doi.org/10.1007/s00232001079, PMID: 10882424

Schlessinger J, Ullrich A. 1992. Growth factor signaling by receptor tyrosine kinases. *Neuron*. **9:**383-391. DOI: https://doi.org/10.1016/0896-6273(92)90177-f, PMID: 1326293

Sharma VK, Li B, Khanna A, Sehajpal PK, Suthanthiran M. 1994. Which way for drug-mediated immunosuppression? *Current Opinion in Immunology* **6:**784-790. DOI: https://doi.org/10.1016/0952-7915(94)90085-x, PMID: 7826535

Shi Y. 2009. Serine/threonine phosphatases: mechanism through structure. *Cell*. **139:**468-484. DOI: https://doi.org/10.1016/j.cell.2009.10.006, PMID: 19879837

Sipos G, Kuchler K. 2006. Fungal ATP-Binding Cassette (ABC) Transporters in Drug Resistance & Detoxification. *Current Drug Targets* **7:**471-481. DOI: https://doi.org/10.2174/138945006776359403, PMID: 16611035

Sirikantaramas S, Yamazaki M, Saito K. 2007. Mechanisms of resistance to self-produced toxic secondary metabolites in plants. *Phytochemistry Reviews* **7:**467-477. DOI: https://doi.org/10.1007/s11101-007-9080-2

Subbarao KV, Chassot A, Gordon TR, Hubbard JC, Bonello P, Mullin R, Okamoto D, Davis RM, Koike ST. 1995. Genetic relationships and cross pathogenicities of

Verticillium dahliae isolates from cauliflower and other crops. *Phytopathology* **85:**1105-1112. DOI: https://doi.org/10.1094/Phyto-85-1105

Sugimoto Y, Ninomiya H, Ohsaki Y, Higaki K, Davies JP, Ioannou YA, Ohno K. 2001. Accumulation of cholera toxin and GM1 ganglioside in the early endosome of Niemann-Pick C1-deficient cells. *PNAS* **98:**12391-12396. DOI: https://doi.org/10.1073/pnas.221181998, PMID: 11675488

Sutton JC. 2009. Epidemiology of wheat head blight and maize ear rot caused by *Fusarium graminearum*. *Canadian Journal of Plant Pathology*. **4:**195-209. DOI: https://doi.org/10.1080/07060668209501326

Tanaka H, Kuroda A, Marusawa H, Hatanaka H, Kino T, Goto T, Hashimoto M, Taga T. 1987. Structure of FK506, a novel immunosuppressant isolated from Streptomyces. *Canadian Journal of Plant Pathology.* **109:**5031-5033. DOI: https://doi.org/10.1021/ja00250a050

Theodoulou FL. 2000. Plant ABC transporters. *Biochim. Biophys. Acta*. **1465:**79-103. DOI: https://doi.org/10.1016/S0005-2736(00)00132-2, PMID: 10748248

Thomson AW, Carroll PB, McCauley J, Woo J, Abu-Elmagd K, Starzl TE, Van Thiel DH. 1993. FK506: a novel immunosuppressant for treatment of autoimmune disease. Rationale and preliminary clinical experience at the University of Pittsburgh. *Seminars in Immunopathology* **14:**323-344. DOI: https://doi.org/10.1007/BF00192307, PMID: 7686690

Tory R, Sachs-Barrable K, Hill JS, Wasan KM. 2008. Cyclosporine A and Rapamycin induce in vitro cholesteryl ester transfer protein activity, and suppress lipoprotein lipase activity in human plasma. *International Journal of*

Pharmaceutics **358:**219-223. DOI: https://doi.org/10.1016/j.ijpharm.2008.03.026, PMID: 18448283

Traber R, Dreyfuss MM. 1996. Occurrence of cyclosporins and cyclosporin-like peptolides in fungi. *Journal of Industrial Microbiology and Biotechnology* **17:**397-401. DOI: https://doi.org/10.1007/BF01574770

Tsuge T, Harimoto Y, Akimitsu K, Ohtani K, Kodama M, Akagi Y, Egusa M, Yamamoto M, Otani H. 2013. Host-selective toxins produced by the plant pathogenic fungus *Alternaria alternata*. *FEMS Microbiology Reviews* **37:**44-66. DOI: https://doi.org/10.1111/j.1574-6976.2012.00350.x, PMID: 22846083

van der Mark VA, Elferink RP, Paulusma CC. 2013. P4 ATPases: flippases in health and disease. *International Journal of Molecular Sciences* **14:**7897-7922. DOI: https://doi.org/10.3390/ijms14047897, PMID: 23579954

van Meer G, Halter D, Sprong H, Somerharju P, Egmond MR. 2006. ABC lipid transporters: extruders, flippases, or flopless activators? *FEBS Letters*. **580:**1171-1177. DOI: https://doi.org/10.1016/j.febslet.2005.12.019, PMID: 16376334

Veronese P, Narasimhan ML, Stevenson RA, Zhu JK, Weller SC, Subbarao KV, Bressan RA. 2003. Identification of a locus controlling Verticillium disease symptom response in *Arabidopsis thaliana*. *The Plant Journal*. **35:**574-587. DOI: https://doi.org/10.1046/j.1365-313x.2003.01830.x, PMID: 12940951

Wang HW, Sun SL, Ge WY, Zhao LF, Hou BQ, Wang K, Lyu ZF, Chen LY, Xu SS, Guo J, Li M, Su P, Li XF, Wang GP, Bo CY, Fang XJ, Zhuang WW, Cheng XX, Wu JW, Dong LH, Chen WY, Li W, Xiao GL, Zhao JX, Hao YC, Xu Y, Gao Y,

Liu WJ, Liu YH, Yin HY, Li JZ, Li X, Zhao Y, Wang XQ, Ni F, Ma X, Li AF, Xu SS, Bai GH, Nevo E, Gao CX, Ohm H, Kong LR. 2020. Horizontal gene transfer of Fhb7 from fungus underlies Fusarium head blight resistance in wheat. *Science*. 368. DOI: https://doi.org/10.1126/science.aba5435, PMID: 32273397

Wang P, Heitman J. 2005. The cyclophilins. *Genome Biology*. **6:**226. DOI: https://doi.org/10.1186/gb-2005-6-7-226, PMID: 15998457

Wolfger H, Mamnun YM, Kuchler K. 2001. Fungal ABC proteins: pleiotropic drug resistance, stress response and cellular detoxification. *Research in Microbiology* **152:**375-389. DOI: https://doi.org/10.1016/s0923-2508(01)01209-8, PMID: 11421285

Xiao G, Ying SH, Zheng P, Wang ZL, Zhang S, Xie XQ, Shang Y, St Leger RJ, Zhao GP, Wang C, Feng MG. 2012. Genomic perspectives on the evolution of fungal entomopathogenicity in *Beauveria bassiana*. *Scientific Reports* **2:**483. DOI: https://doi.org/10.1038/srep00483, PMID: 22761991

Zhang BL, Yang YW, Chen TZ, Yu WG, Liu TL, Li HJ, Fan XH, Ren YZ, Shen DY, Liu L, Dou DL, Chang YH. 2012. Island cotton Gbve1 gene encoding a receptor-like protein confers resistance to both defoliating and non-defoliating isolates of *Verticillium dahliae*. *PLoS One*. **7:**e51091. DOI: https://doi.org/10.1371/journal.pone.0051091, PMID: 23251427

Zhang SZ, Fan YH, Xia YX, Keyhani NO. 2010. Sulfonylurea resistance as a new selectable marker for the entomopathogenic fungus *Beauveria bassiana*. *Applied Microbiology and Biotechnology* **87:**1151-1156. DOI: https://doi.org/10.1007/s00253-010-2636-x, PMID: 20449738

Zhou L, Zhao J, Guo WZ, Zhang TZ. 2013. Functional analysis of autophagy genes *via Agrobacterium-mediated* transformation in the vascular Wilt fungus *Verticillium dahliae*. *Journal of Genetics and Genomics* **40:**421-431. DOI: https://doi.org/10.1016/j.jgg.2013.04.006, PMID: 23969251

Zhou XM, Graham TR. 2009. Reconstitution of phospholipid translocase activity with purified Drs2p, a type-IV P-type ATPase from budding yeast. *PNAS* **106:**16586-16591. DOI: https://doi.org/10.1073/pnas.0904293106, PMID: 19805341

Zhou YH, Keyhani NO, Zhang YJ, Luo ZB, Fan YH, Li YJ, Zhou QS, Chen JJ, Pei Y. 2016. Dissection of the contributions of cyclophilin genes to development and virulence in a fungal insect pathogen. *Environmental Microbiology***18:**3812-3826. DOI: https://doi.org/10.1111/1462-2920.13339, PMID: 27130487

Supplement figure legends:

Figure 1-figure supplement 1. *B. bassiana* shows resistance to CsA and FK506 and identification of CsA-sensitivity mutants, *mu*1 and *mu*2.

(A and B) *B. bassiana* shows resistance to CsA (A) and FK506 (B), while some other filamentous fungi tested show sensitivity to them. 1, *Beauveria bassiana*; 2, *Metarhizium anisopliae*; 3, *Botrytis cinerea*; 4, *Alternaria brassicae*; 5, *Alternaria brassicicola*; 6, *Aspergillus nidulans*; 7, *Alternaria solani*. CsA/FK506 was diluted with dimethyl sulfoxide (DMSO) in the concentrations of 1000 μg/ml, 100 μg/ml, 10 μg/ml, 0 μg/ml. Petri-dishes (90 mm) containing PDA (20 ml) mixed with 100 μl conidial suspensions (1×10^7 conidia/ml in 0.05% Tween-80) were incubated at 26 °C

for 4-7 days. Each hole (5-mm diameter) was filled with 5 μl different concentrations of CsA/FK506. All inhibition assays were performed thrice. **(C and D)** *mu*1 and *mu*2 show sensitivity to CsA. The wild-type, *mu*1, and *mu*2 strains were grown on CZP + CsA (20 μg/ml). Plates were spot inoculated with 3 μl conidial suspensions (1×10^7 conidia/ml) and incubated at 26 °C for about 10 days. The variation in growth rates were shown as [colony diameter CZP supplemented with CsA]/[colony diameter CZP]. All experiments were performed in triplicate. Scale bar, 1 cm. Data are represented as mean ± SD. ****$p < 0.0001$ from Student's *t* test. **(E)** Sequencing of the T-DNA insertion junctions in CsA-sensitive mutant *mu*1 and *mu*2. The top line shows the left and the right border sequences of T-DNA from plasmid vector pK2, respectively; the red uppercase letters denote nucleotides of T-DNA border conserved sequences; the green uppercase letters denote overlapping sequences; flanking genomic sequences are indicated by lowercase letters; "…"denotes *Bar*::*Gus* element in T-DNA, "*" denotes the T-DNA border imperfect sequences; sequence data for *mu*1 (right border) was not obtained, and is indicated by "×". **(F)** Cluster analysis indicates that BbCrpa belongs to P-type ATPase superfamily of P4 branch (P4-ATPases). BbCrpa orthologues were aligned with CLUSTALW (MEGA5.2) based on its amino acid sequences. Ca, *Candida albicans*; Cm, *Cordyceps militaris*; Ec, *Escherichia coli*; Fo, *Fusarium oxysporum*; Ma, *Metarhizium anisopliae*; Mo, *Magnaporthe oryzae*; Mr, *Metarhizium robertsii*; Nc, *Neurospora crassa*; Sc, *Saccharomyces cerevisiae*; Vd, *Verticillium dahliae*. **(G)** The phosphorylated Asp in BbCrpa (red) is situated in the conserved sequence DKTG as other P4-ATPases. Aa, *Acremonium chrysogenum*; Af,

Aspergillus fumigatus; An, *Aspergillus nidulans*; Bb, *Beauveria bassiana*; Ca, *Candida albicans*; Cp, *Claviceps purpurea*; Ch, *Colletotrichum higginsianum*; Co, *Colletotrichum orbiculare*; Cm , *Cordyceps militaris*; Ff, *Fusarium fujikuroi*; Mo, *Magnaporthe oryzae*; Ma1, *Metarhizium acridum*; Ma2, *Metarhizium anisopliae*; Mr, *Metarhizium robertsii*; Nh, *Nectria haematococca*; Nc, *Neurospora crassa*; Os, *Ophiocordyceps sinensis*; Op, *Ophiostoma piceae*; Sc, *Saccharomyces cerevisiae*; Sa, *Scedosporium apiospermum*; Th, *Torrubiella hemipterigena*; Ta, *Trichoderma atroviride*; Uv, *Ustilaginoidea virens*; Vd, *Verticillium dahliae*. **(H)** Predicted topological model of BbCrpa. The topological map was forecasted by https://embnet.vital-it.ch/software/TMPRED_form.html and https://services.healthtech.dtu.dk/service.php?TMHMM-2.0. BbCrpa consists of 10 transmembrane-spanning segments. A-domain, actuator domain; P-domain, phosphorylation domain; N-domain, nucleotide binding domain; aa, amino acid.

The following source data is for figure 1-figure supplement 1:

Source data 1. Growth of WT, *mu*1 and *mu*2 at CZP supplemented with CsA normalized to growth at CZP.

Figure 1-figure supplement 2. Construction and Identification of *BbCRPA* disruption strain.

(A) Schematic model of construction for *BbCRPA* gene replacement vector. **(B)** PCR analysis of *BbCRPA* disruption mutant (M, DNA Marker DL2000; 1, PCR product of plasmid vector; 2, PCR product of *BbCRPA* disruption mutant (Δ*BbCRPA*); 3, PCR product of wide-type *B.bassiana* (WT); 4, PCR product of heterologous recombinant

mutant). **(C)** The expression level of *BbCRPA* in the wild-type, Δ*BbCRPA* and the complementary strain (Δ*BbCRPA*::*BbCRPA*). **(D and E)** Disruption of *BbCRPA* makes *B. bassiana* sensitive to FK506. **(F and G)** Disruption of *BbCRPA* renders growth defect of *B. bassiana*. **(H)** Knock out *BbCRPA* has no significant effect on the conidial germination rate of *B.bassiana*. Conidial germination was monitored *via* microscopic analysis. Conidia were considered germinated when the germ tube was equal in length to the half diameter of the conidia. About 300 conidia were examined for the wide-type and Δ*BbCRPA*. All experiments were performed in triplicate on CZP medium. **(I)** Loss of *BbCRPA* has no significant effect on the conidial yield of *B.bassiana*. Conidia of the fungal strains on CZA medium were harvested after 14 days at 26 °C. All experiments were performed in triplicate. **(J)** Knock out *BbCRPA* reduces the virulence of *B.bassiana*. Survival of *Galleria mellonella* larvae treated with suspensions (2×10^7 conidia/ml in 0.05% tween-80) derived from the wild-type, *BbCRPA* disruption mutant. Control was treated with tween-80 alone. Survival curves were plotted by using the Kaplan-Meier method and a log rank test was used to analyse the difference between Δ*BbCRPA* and the wild-type. **(K and L)** Converting Ile to Glu at the site of 562 and Asp to Arg at the site of 614 both disrupt the function of BbCrpa. **(M and N)** Expression *DRS2* in Δ*BbCRPA* was unable to recover the resistance of *B.bassiana* to CsA. For CsA/FK506 sensitivity analysis, plates were spot inoculated with 3 μl conidial suspensions (1×10^7 conidia/ml) and incubated at 26 ^{o}C for about 10 days. The variation in growth rates were shown as [colony diameter CZP supplemented with CsA]/[colony diameter CZP]. All experiments were performed in

triplicate. Scale bars, 1 cm for (**D, F, K, and M**). Data are represented as mean ± SD. ***p < 0.001, ****p < 0.0001 from Student's *t* test. NS, not significant.

The following source data is for figure 1-figure supplement 2:

Source data 1. qRT-PCR experiments, conidial yield, and growth of target strains at CZP supplemented with CsA normalized to growth at CZP.

Figure 2-figure supplement 1. Fluorescent-labeled CsA and FK506 maintain their toxic activity.

(A and B) The fluorescein-labeled CsA (CsA-5-FAM) maintains biological activity. The wild-type and Δ*BbCRPA* strains were grown on CZP, CZP + 5-FAM (32.7 μM), CZP + CsA (32.7 μM), CZP + CsA-5-FAM (32.7 μM). **(C and D)** The fluorescein-labeled FK506 (FK506-5-FAM) maintains biological activity. The wild-type and Δ*BbCRPA* strains were grown on CZP, CZP + 5-FAM (42.4 μM), CZP + FK506 (42.4 μM), CZP + FK506-5-FAM (42.4 μM). For CsA-5-FAM/FK506-5-FAM sensitivity analysis, plates were spot inoculated with 3 μl conidial suspensions (1×10^7 conidia/ml) and incubated at 26 °C for about 10 days. Different strains showed variation in growth rates and the data were shown as [colony diameter CZP supplemented with CsA/FK506/5-FAM/CsA-5-FAM/FK506-5-FAM]/[colony diameter CZP]. Scale bars, 1 cm for (A and C). Data are represented as mean ± SD. ****p < 0.0001 from Student's *t* test.

The following source data is for figure 2-figure supplement 1:

Source data 1. Growth of target strains at CZP supplemented with 5-FAM/CsA/FK506/CsA-5-FAM/FK506-5-FAM normalized to growth at CZP.

Figure 3-figure supplement 1. BbCrpa N-terminally tagged with eGFP maintains its original function and is localized to the apical plasma membrane and

Spitzenkörper of *B. bassiana.*

(A) Schematic diagram of eGFP::BbCrpa fusion protein. **(B and C)** Expression *eGFP*::*BbCRPA* fusion gene in Δ*BbCRPA* strain could restore the resistance to CsA. **(D and E)** eGFP was fused to other 9 different sites of BbCrpa. TMD, transmembrane segments; aa, amino acid. **(F and G)** Complementary experiments (expression all the 9 constructs of *eGFP-BbCRPA* fusion genes in Δ*BbCRPA* strain) showed that four fusions of eGFP with BbCrpa, i.e., at the sites of C-terminus (T2), and the putative outside-membrane region between transmembrane segments 4 and 5 (M2), 8 and 9 (M7), and 9 and 10 (M8) did not compromise the property of BbCrpa. **(H)** eGFP::BbCrpa localizes to the apical plasma membrane (arrows) and cytosolic structures stained with FM4-64 in germinating conidia. **(I)** eGFP::BbCrpa localizes to the Spitzenkörper (arrows) stained by FM4-64 in germ tubes. **(J)** mRFP::BbRab5 colocalizes with FM1-43 signal in early endosomes (LEs, white arrows) and in vacuoles (red arrows). **(K)** mRFP::BbRab7 colocalizes with FM1-43 signal in late endosomes (LEs, arrows). **(L)** mRFP::BbCrpa appears in vesicles (white arrows) and vacuoles (red arrows), the membranes of which are indicated by FM1-43. For CsA sensitivity analysis, plates were spot inoculated with 3 μl conidial suspensions (1×10^7 conidia/ml) and incubated at 26 °C for about 10 days. Different strains showed variation in growth rates and the data were shown as [colony diameter CZP supplemented with CsA]/[colony diameter CZP]. Scale bars, 1 cm for (B and F) and 5 μm for (**H**-**L**). Data are represented as mean ± SD. ****$p < 0.0001$ from Student's *t* test. NS, not significant.

The following source data is for figure 3-figure supplement 1:

Source data 1. Growth of target strains at CZP supplemented with CsA normalized to growth at CZP.

Figure 4-figure supplement 1. Y1325 (Tyr) in C-terminus is critical for detoxification of FK506, and the N-terminus is essential for vacuolar targeting. **(A and B)** BbCrpa C-terminus Y1325 is critical for detoxification of FK506. All strains were incubated in CZP + FK506 (20 μg/ml). **(C and D)** BbCrpa N- and C-terminus are crucial for its detoxification activity. All strains were incubated in CZA + FK506 (20 μg/ml). **(E)** BbCrpa N-terminus contains vacuolar sorting signal. dB^{N}, Deleting N-terminus of BbCrpa; dB^{C}, Deleting C-terminus of BbCrpa. **(F)** The fusions of mRFP with different sizes of BbCrpa N-terminus ($B^{N151-268}$, $B^{N216-268}$, $B^{N226-268}$, $B^{N236-268}$, $B^{N246-268}$, $B^{N256-268}$, and $B^{N257-268}$) are obviously colocalized with BbCrpa in vacuoles (arrows). **(G)** K264 is responsible for the ubiquitination of $B^{N258-268\ (K264A)}$::mRFP. Total extracts of the strains were incubated with anti-RFP affinity beads 4FF. After intensive washing, the IP materials (anti-RFP) were subjected to immunoblot with anti-Ub (ubiquitin) and anti-RFP antibodies. The total extracts (input) were detected by immunoblot with anti-RFP antibody. +: CsA (20 μg/ml), -: DMSO. For FK506 sensitivity analysis, plates were spot inoculated with 3 μl conidial suspensions (1×10^7 conidia/ml) and incubated at 26 °C for about 10 (CZP/CZP + CsA) or 14 (CZA/CZA + CsA) days. The variation in growth rates was shown as [colony diameter CZP/CZA supplemented with CsA]/[colony diameter CZP/CZA]. All experiments were performed in triplicate. Data are represented as mean ± SD. **p < 0.01; ***p < 0.001; ****p < 0.0001 from Student's *t* test. NS, not significant. Scale bars, 1 cm for (A and C) and 5 μm for (**E and F**).

The following source data are for figure 4-figure supplement 1:

Source data 1. Growth of target strains at CZP/CZA supplemented with FK506 normalized to growth at CZP/CZA.

Source data 2. Uncropped western blot.

Figure 5-figure supplement 1. Validation of transgenic *BbCRPA* plants.

(**A and D**) PCR validation of *BbCRPA* transcription in transgenic Arabidopsis (**A**) and cotton (**D**). M, DNA Marker DL2000. (**B and E**) Transcriptional level detection of *BbCRPA* in transgenic Arabidopsis (**B**) and cotton (**E**) plants by qRT-PCR. (**C and F**) Southern blot validation of *BbCRPA* insertions in transgenic Arabidopsis (**C**) and cotton (**F**). Genomic DNA was digested with *Hin*dIII and then hybridized with a 912 bp DNA probe produced *via* PCR from *BbCRPA*. Southern blot results indicate *35S::BbCRPA*-1 Arabidopsis line holds two copies, while *35S::BbCRPA*-12 line has single copy of transgene; *35S::BbCRPA*-B1 cotton line has single copy, while *35S::BbCRPA*-B56 line has two copies of transgene. M, DNA Molecular Weight Marker III; plasmid, positive control fragment from modified pCAMBIA2300 (PLGN).

The following source data are for figure 5-figure supplement 1:

Source data 1. qRT-PCR

Source data 2. Southern blot.

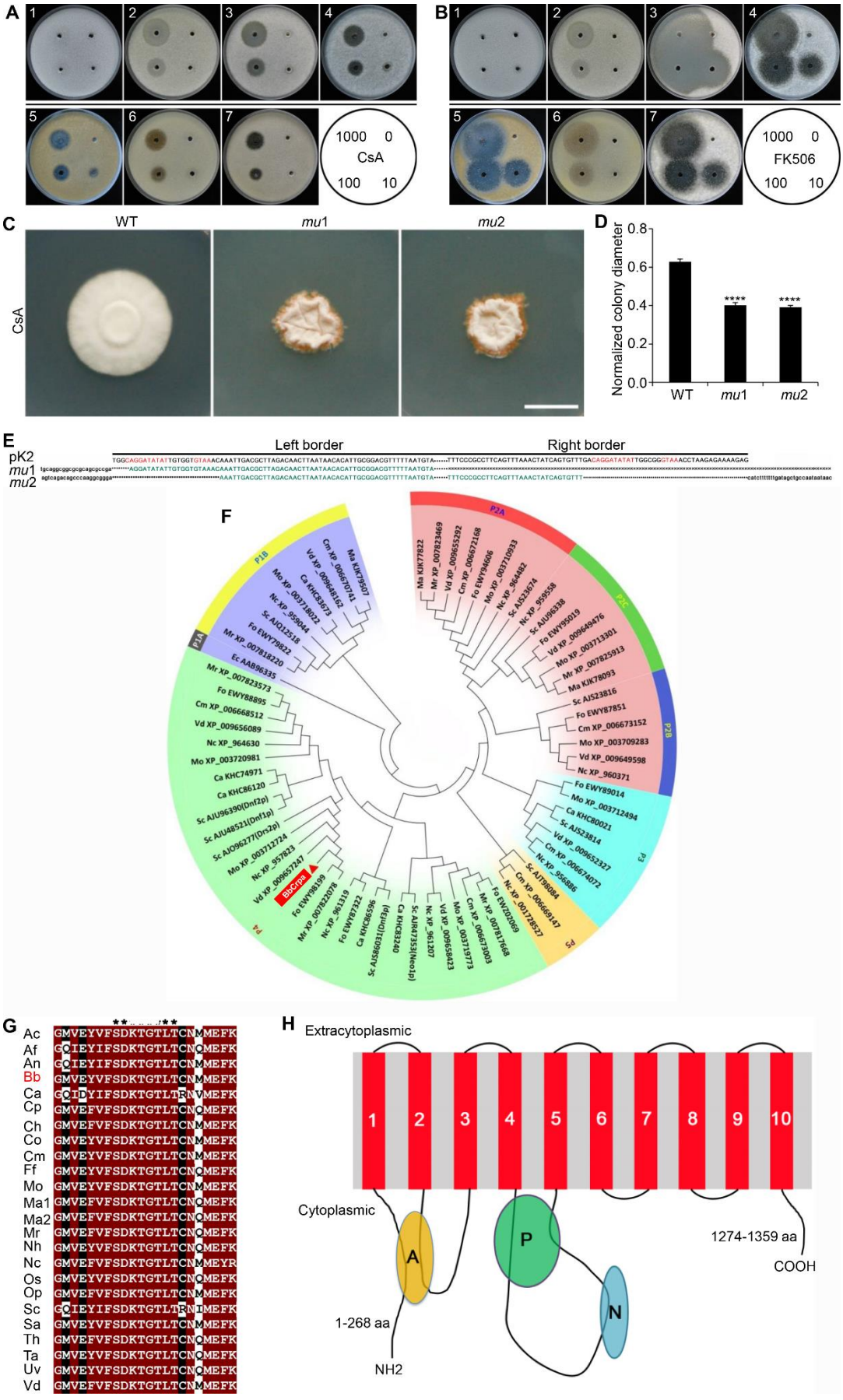

1422 **Figure 1-figure supplement 1**

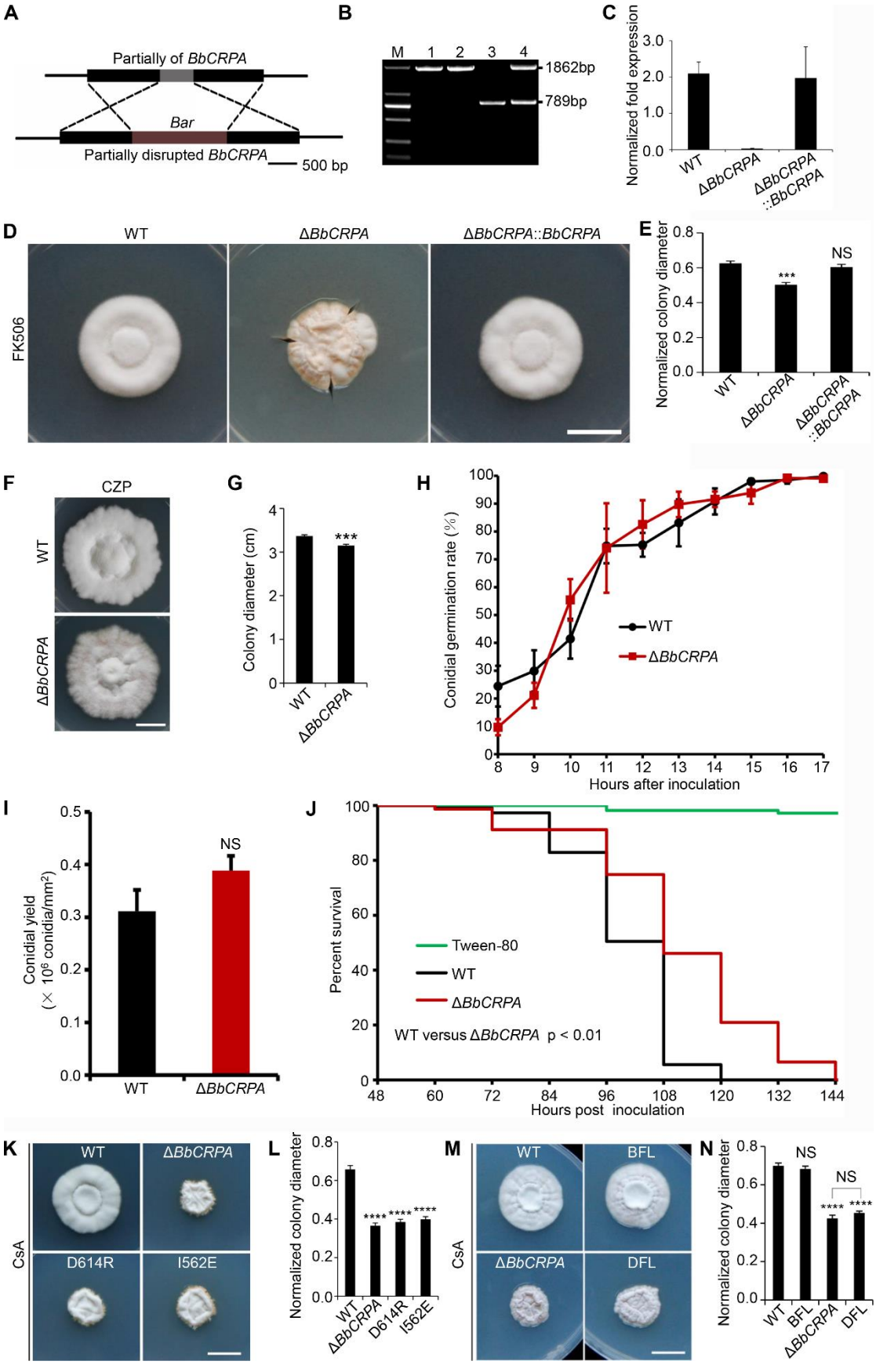

1423 **Figure 1-figure supplement 2**

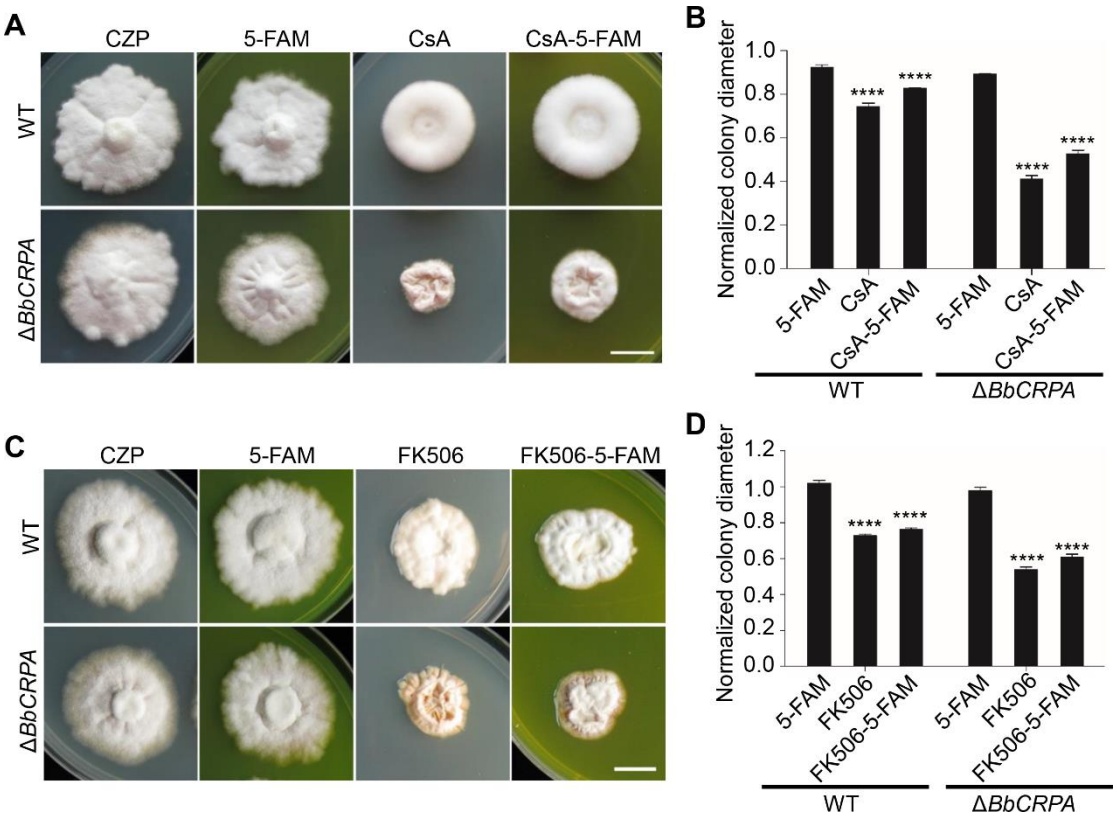

1424 **Figure 2-figure supplement 1**

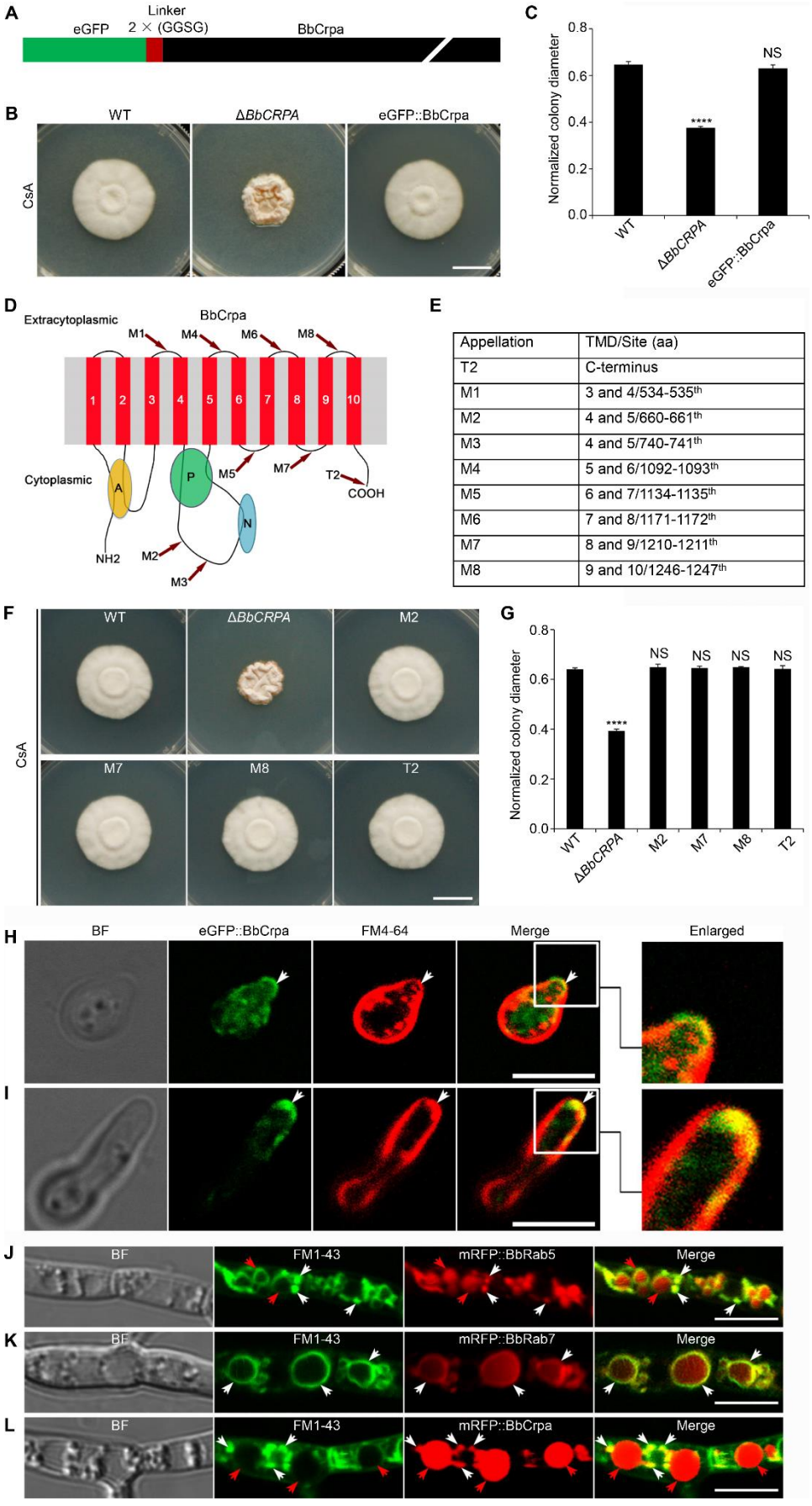

Appellation	TMD/Site (aa)
T2	C-terminus
M1	3 and 4/534-535th
M2	4 and 5/660-661th
M3	4 and 5/740-741th
M4	5 and 6/1092-1093th
M5	6 and 7/1134-1135th
M6	7 and 8/1171-1172th
M7	8 and 9/1210-1211th
M8	9 and 10/1246-1247th

Figure 3-figure supplement 1

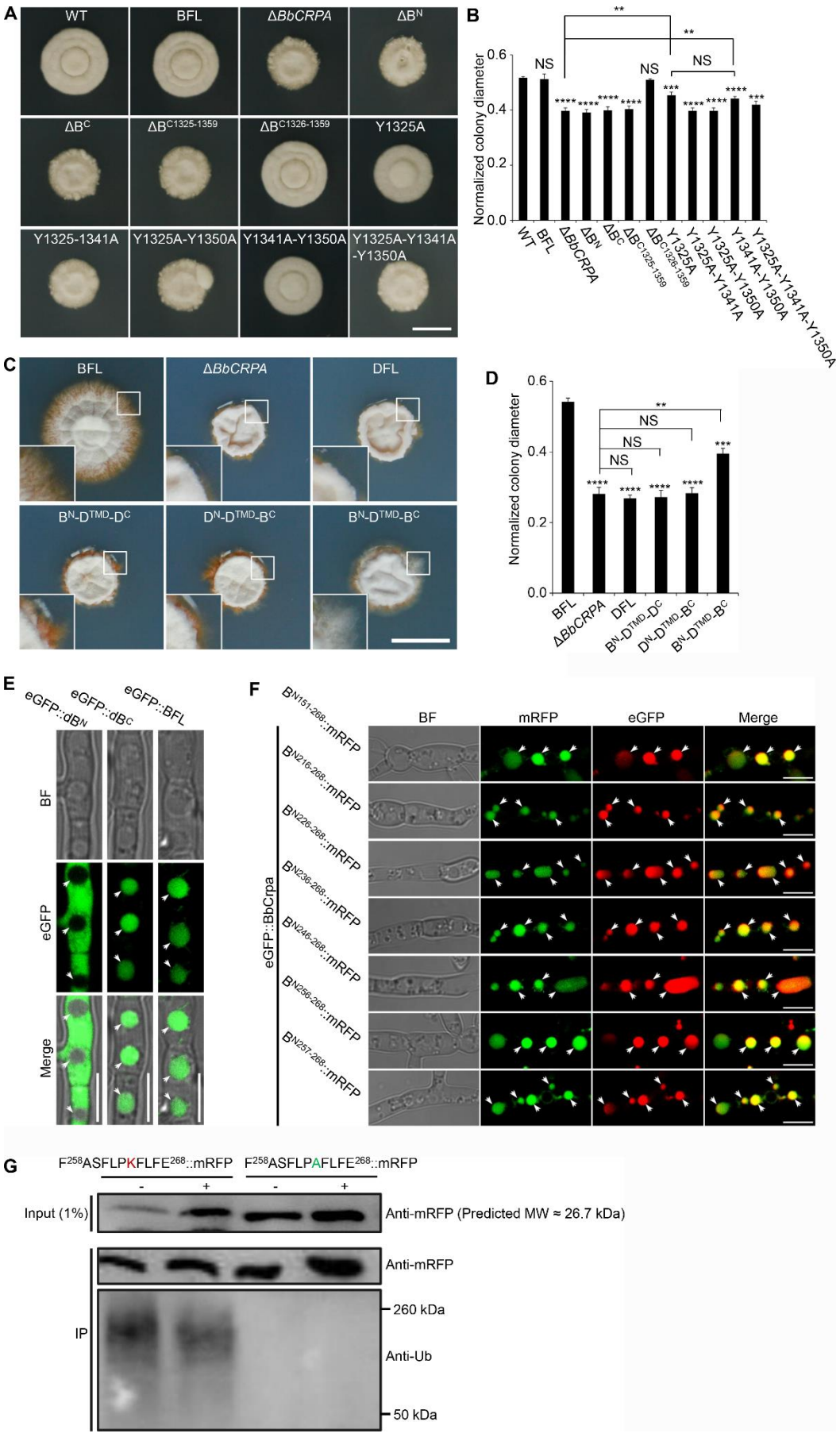

1426 **Figure 4-figure supplement 1**

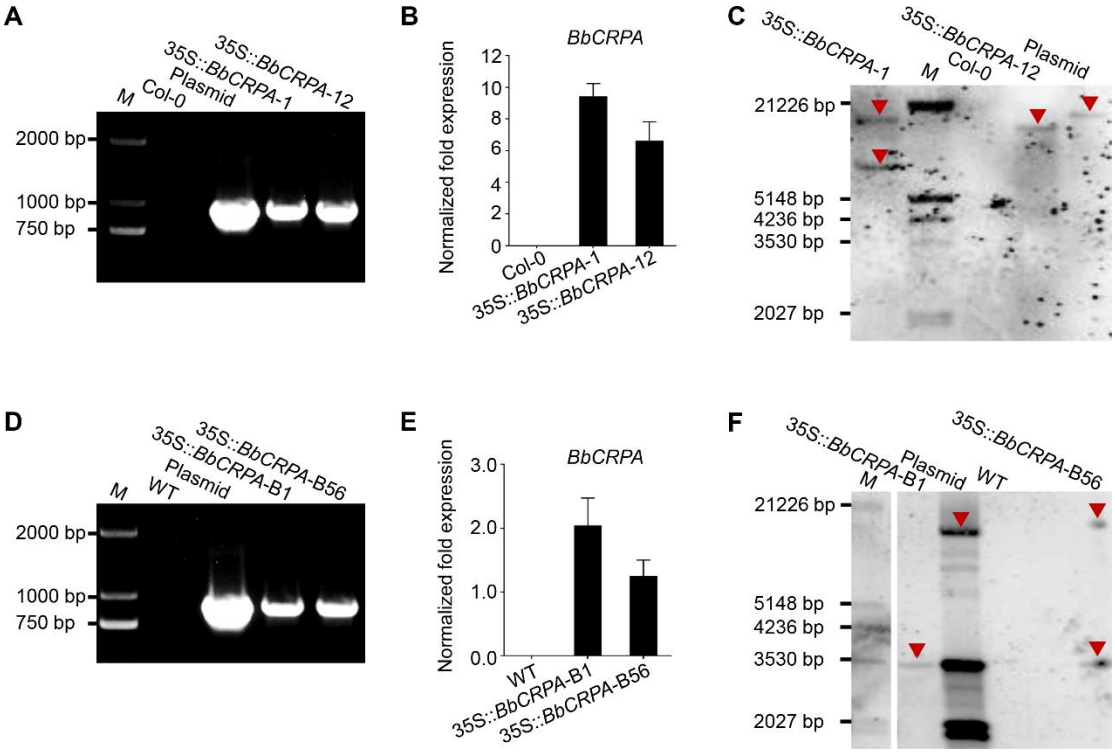

1427 **Figure 5-figure supplement 1**

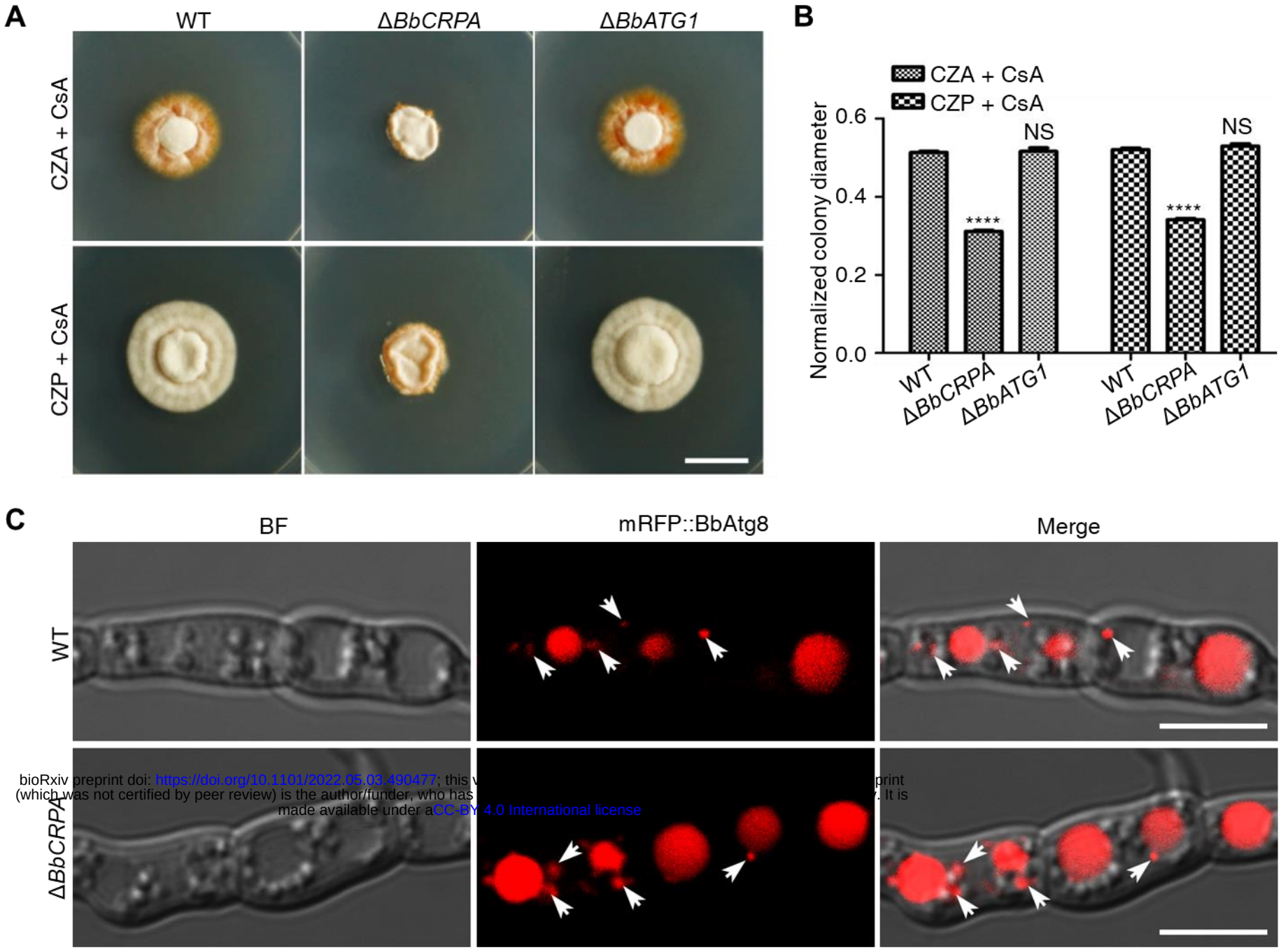

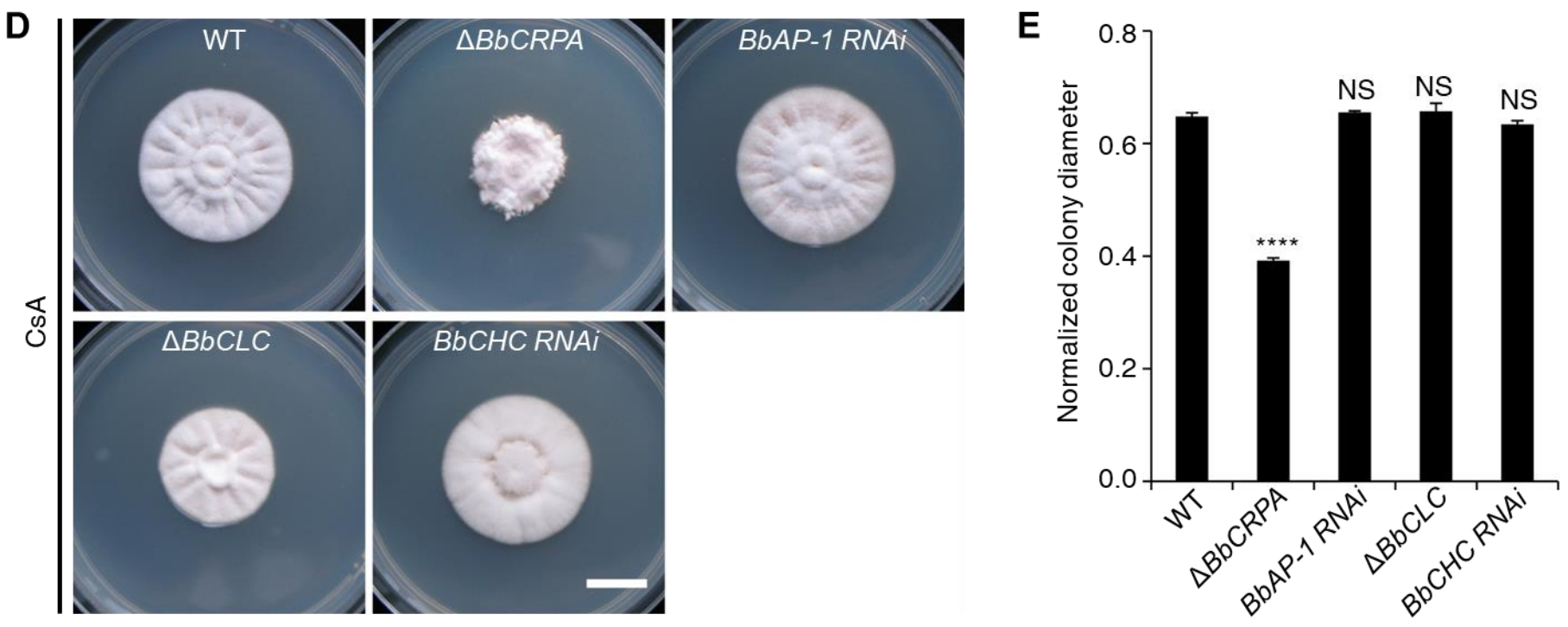

Supplementary file 3. Loss of autophagy-related protein BbAtg1, adaptor protein BbAP-1, or coat protein clathrin does not affect CsA resistance. **(A and B)** Growth of the wild-type, Δ*BbCRPA*, and Δ*BbATG1* strains on CZA/CZP + CsA (20 μg/ml). **(C)** Disruption of *BbCRPA* does not affect the autophagosome formation in *B. bassiana*. Autophagosomes are marked by mRFP::BbAtg8 (arrows). **(D and E)** Growth of the wild-type, Δ*BbCRPA*, *BbAP-1 RNAi*, Δ*BbCLC*, and *BbCHC* strains on CZP + CsA (20 μg/ml). CLC, clathrin light chain; CHC, clathrin heavy chain. For CsA sensitivity analysis, plates were spot inoculated with 3 μl conidial suspensions (1×10^7 conidia/ml) and incubated at 26 °C for about 10 days. Different strains showed variation in growth rates and the data were shown as [colony diameter CZP supplemented with CsA]/[colony diameter CZP] in (**B**). Scale bars, 1 cm for (**A and D**) and 5 μm for (**C**). Data are represented as mean ± SD. ****$p < 0.0001$ from Student's *t* test. NS, not significant.

The following source is for supplementary file 3:

Source data 1. Growth of target strains at CZP/CZA supplemented with CsA normalized to growth at CZP/CZA.